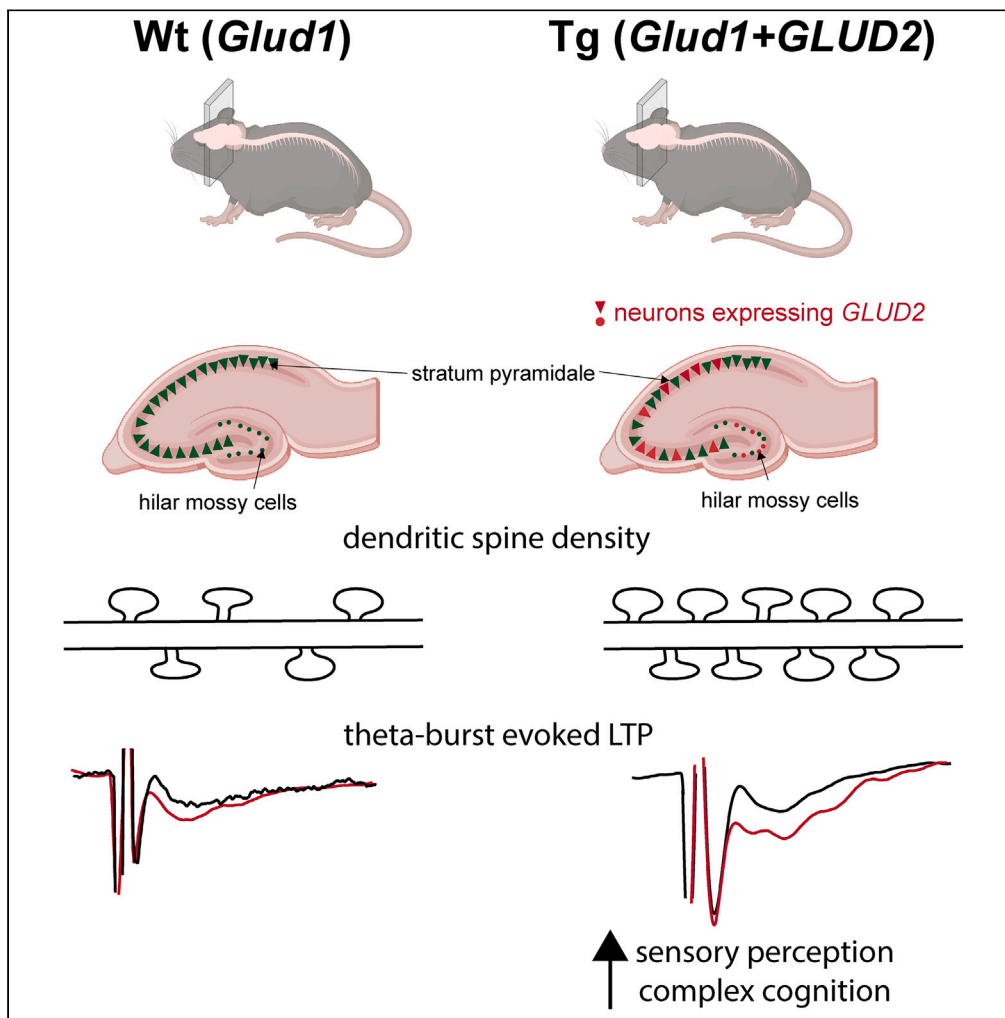


Article

Glutamate-specific gene linked to human brain evolution enhances synaptic plasticity and cognitive processes



Cleanthe Spanaki, Kyriaki Sidiropoulou, Zoe Petraki, ..., Konstantina Mylonaki, Maria Savvaki, Andreas Plaitakis

kliospanaki@gmail.com (C.S.)
andreasplaitakis@gmail.com (A.P.)

Highlights
Transgenic mice express *GLUD2* in hippocampal (CA1-CA3) pyramidal neurons and astrocytes

LTP is markedly enhanced in CA3/CA1 synapses via a lactate-dependent mechanism

GLUD2 augments synaptic plasticity by enhancing NMDA receptor currents

Dendritic spine density, sensory perception and complex cognitive functions are enhanced

Spanaki et al., iScience 27, 108821
February 16, 2024 © 2024 The Authors.
<https://doi.org/10.1016/j.isci.2024.108821>



Article

Glutamate-specific gene linked to human brain evolution enhances synaptic plasticity and cognitive processes

Cleanthe Spanaki,^{1,4,5,*} Kyriaki Sidiropoulou,^{2,3,5} Zoe Petraki,¹ Konstantinos Diskos,^{2,3} Xanthippi Konstantoudaki,² Emmanouela Volitaki,^{1,2} Konstantina Mylonaki,¹ Maria Savvaki,¹ and Andreas Plaitakis^{1,6,*}

SUMMARY

The human brain is characterized by the upregulation of synaptic, mainly glutamatergic, transmission, but its evolutionary origin(s) remain elusive. Here we approached this fundamental question by studying mice transgenic (Tg) for *GLUD2*, a human gene involved in glutamate metabolism that emerged in the hominoid and evolved concomitantly with brain expansion. We demonstrate that Tg mice express the human enzyme in hippocampal astrocytes and CA1-CA3 pyramidal neurons. LTP, evoked by theta-burst stimulation, is markedly enhanced in the CA3-CA1 synapses of Tg mice, with patch-clamp recordings from CA1 pyramidal neurons revealing increased sNMDA currents. LTP enhancement is blocked by D-lactate, implying that *GLUD2* potentiates L-lactate-mediated astrocyte-neuron interaction. Dendritic spine density and synaptogenesis are increased in the hippocampus of Tg mice, which exhibit enhanced responses to sensory stimuli and improved performance on complex memory tasks. Hence, *GLUD2* likely contributed to human brain evolution by enhancing synaptic plasticity and metabolic processes central to cognitive functions.

INTRODUCTION

The human brain is distinguished from that of the non-human primates by its large size and high rates of neuronal activity and energy utilization.¹ Thus, large-scale expression studies have demonstrated the elevated expression of proteins involved in synaptic transmission and energy metabolism,² with the glutamatergic signaling pathway being the selective target of human brain evolution.³ This is not surprising, given that the neural circuits that sub-serve cognitive functions are made primarily of pyramidal neurons utilizing glutamate as their excitatory transmitter and that glutamatergic transmission accounts for about 60–80% of energy provided by glucose oxidation in human cerebral cortex.⁴ The central role of the glutamatergic transmission in cognitive functions is underscored by observations showing that high frequency excitatory stimulation leads to the long-lasting strengthening of synaptic responses or long-term potentiation (LTP) and synaptic remodeling (structural plasticity).⁵

While the glutamate signaling pathway is upregulated in human brain, the underlying mechanisms driving these adaptations remain largely unknown. At the genomic level, the protein coding sequences of genes involved in synaptic transmission (including those for glutamate receptors) did not undergo accelerated evolution, although changes have taken place in non-coding sequences involved in gene regulation.^{6–8} Moreover, glutamate metabolism underwent significant evolutionary changes via the emergence of the *GLUD2* gene⁹ in the common ancestor of humans and great apes.¹⁰ The novel gene encodes the hGDH2 isoform of glutamate dehydrogenase, a mitochondrial enzyme involved in synaptic glutamate and energy metabolism¹¹ that evolved concomitantly with human brain expansion.¹⁰ Its genesis may relate to selective pressures on the genome to enhance excitatory mechanisms required for the expansion of the cognitive capabilities of the Hominidae.¹²

Previous studies have established that *GLUD2* arose through the retro-positioning of a processed *GLUD1* mRNA to the Xq chromosome,⁹ where under the influence of a novel promoter gained expressional diversification.¹² Importantly, driven by positive Darwinian selection, *GLUD2* underwent rapid evolutionary adaptation acquiring 15 amino acid changes.⁹ These evolutionary substitutions provided hGDH2 with unique functional properties that permit enhanced catalytic function under conditions inhibitory to its ancestor hGDH1 (encoded by

¹Department of Neurology, School of Health Sciences, University of Crete, Voutes, Iraklion, Crete, Greece

²Department of Biology, University of Crete, Voutes, Iraklion, Crete, Greece

³Institute of Molecular Biology and Biotechnology, Foundation for Research and Technology Hellas (IMBB-FORTH), Iraklion, Greece

⁴PaGNI University Hospital of Irakleio, Neurology Department, Iraklion, Crete, Greece

⁵These authors contributed equally

⁶Lead contact

*Correspondence: kliospanaki@gmail.com (C.S.), andreasplaitakis@gmail.com (A.P.)

<https://doi.org/10.1016/j.isci.2024.108821>



the *GLUD1* gene).¹³ Notably, the novel regulatory pattern of hGDH2 (marked ADP activation dissociated from GTP inhibition) enables enzyme recruitment under conditions of intense glutamatergic transmission associated with high energy utilization (increased the conversion of ATP to ADP).¹⁴ Indeed, the transgenic expression of hGDH2 in astrocytes augments the capacity of the TCA cycle and that of glutamate uptake/metabolism, particularly when glutamate concentrations approach those present in the synaptic cleft during intense glutamatergic firing.¹⁵ In spite of this progress, the selective advantage provided to humans by this positive selected gene remains unclear. To better understand the potential role of these recent genomic changes in human biology, we generated transgenic (Tg) mice carrying the *GLUD2* gene in their genome¹² and used them to investigate the effect of the human gene on structural, physiological and behavioral aspects of cognitive function.

RESULTS

***GLUD2* is expressed in hippocampal CA1-CA3 pyramidal cells and hilar mossy-like cells, neurons crucial to memory processes**

We used transgenic mice (Tg) carrying the *GLUD2* gene and its regulatory elements to study the expression of the human gene in the host brain. The Tg mice were constructed by inserting a BAC clone, containing a 176.6 kb fragment of the human X chromosome (encompassing the *GLUD2* gene along with a 40 kb of upstream and 135 kb of downstream DNA sequences) in their genome.¹² Two *GLUD2* Tg lines (Tg13 and Tg32), constructed independently, were used for these studies. The *GLUD2* Tg mice grew normally reaching advanced age (24 months) without exhibiting apparent untoward effects.

Immunoblots of brain homogenates, obtained from Tg mice and their wild-type (Wt) littermates, were probed by antibodies specific for either the human hGDH2 protein or the endogenous GDH1 enzyme.¹² The blots reveal that hGDH2 is expressed in the hippocampus and in the cerebral cortex of Tg animals, with similar levels of hGDH2 expression being detected in each of our two Tg lines (Tg13 and Tg32) (Figure 1A). On the other hand, the Wt mice, known to possess the single mammalian *Glud1* gene, express the mouse GDH1 (mGDH1) protein only (Figure 1A). Expression of the human hGDH2 protein in the brain of the Tg mice does not affect the levels of the endogenous mouse mGDH1 (Figure 1A).

Using immunofluorescence (IF)-confocal microscopy we find that hGDH2 is expressed in the hippocampus of the Tg mice in a laminated-like pattern, with the stratum lacunosum moleculare (SLM), stratum oriens (SO) and stratum pyramidale (SP) being prominently labeled (Figure 1B; Figure S1). Double IF experiments using our anti-hGDH2 antibody (green) and another against NeuN (a neuronal marker) (red) reveal the colocalization of the two proteins in the CA1-CA3 regions of the stratum pyramidale (SP) (appearing yellow in merge images) (Figure 1B). Here, the pyramidal cells of the CA1-CA3 regions are intensively labeled by the anti-hGDH2 antibody (appearing yellow in merged images) (Figures 1C–1F; Figure S2). The hGDH2-specific labeling is punctate-like, as expected from the mitochondrial localization of the human protein, and is distributed in the perikaryon of the pyramidal neurons (Figures 1D and 1F; Figure S2). In these cells, large hGDH2-specific “puncta” are detected (Figures 1E and 1F; Figure S2), which are quite similar to those observed in human brain.¹⁶ GDH2-specific expression is also detected in some of the hilar mossy-like cells located in the sub-granular area of the dentate gyrus (DG) (Figures 1G and 1H; Figure S1). In contrast, the granule cells lack hGDH2-specific labeling (Figures 1B and 1I; Figure S1). Regarding hGDH2 expression in glial cells, punctate-like, hGDH2-specific labeling is seen throughout the neuropil of the hippocampus, including that of the granule cell (GC) layer, the molecular layer (ML) and the hilus (HL) of DG. In all these regions, including the stratum radiatum (SR) that harbors the CA3-CA1 synapses, hGDH2 localizes to GFAP-positive astrocytes (Figures 1I and 1J; Figure S3). In the corresponding regions of the Wt mice brain, our anti-hGDH2 antibody does not recognize any of the structures labeled by this antibody in Tg mice brain, thus confirming the specificity of the antibody (Figures S2 and S3).

Our present observations, showing that hGDH2 localizes to hippocampal pyramidal neurons and astrocytes, are consistent with previous investigations on human and Tg mouse cerebral cortex, which revealed that the enzyme is expressed in nerve cells with pyramidal morphology, in addition to being expressed in glial cells.^{12,16} To gain further insight into the CNS *GLUD2* expression pattern, we studied here the cerebellar cortex, which lacks pyramidal neurons. We observe hGDH2 expression in the Bergman Glia cells (located of in the Purkinje cell layer) and their processes inside the molecular layer, and in the neuropil that surrounds the numerous granule cells (Figure S4). In contrast, none of the cerebellar cortical neurons (granule cells, Purkinje cells, basket, and stellate cells) is found to express the human enzyme (Figure S4).

Here we demonstrate that the human *GLUD2* gene, driven by its natural promoter and other regulatory elements contained in the segment of the human X chromosome used to construct our two Tg lines, is expressed in the host hippocampus in astrocytes and in neurons crucial to cognitive functions. Expression of hGDH2 in pyramidal neurons, large cells exhibiting complex anatomical and functional features that correlate with the evolution of human cognitive abilities¹⁷ suggest an important role for the newly evolved human enzyme in the biology of these cells. In light of these considerations and, given the role of hippocampal pyramidal neurons in memory processes, we next investigated the effect of the transgenic expression of *GLUD2* on the synaptic activity of these cells and on the cognitive functions that are dependent on these neurons.

***GLUD2* potentiates excitatory transmission and synaptic plasticity in the hippocampus**

As the present morphological data reveal that hGDH2 is expressed in hippocampal glutamatergic neurons crucial to information processing and storage, we explored whether *GLUD2* expression modulates synaptic strength by studying excitatory transmission and long-term potentiation (LTP) in hippocampal slices. Results revealed that LTP, evoked by theta-burst stimulation, is significantly enhanced in the CA3-CA1 synapses of Tg mice as compared to their Wt littermates (Figure 2). Specifically, we find that the field Evoked Excitatory PostSynaptic Potentials (fEPSP) recorded from the CA1 region following the stimulation of Schaffer collaterals are significantly increased in Tg mice as compared

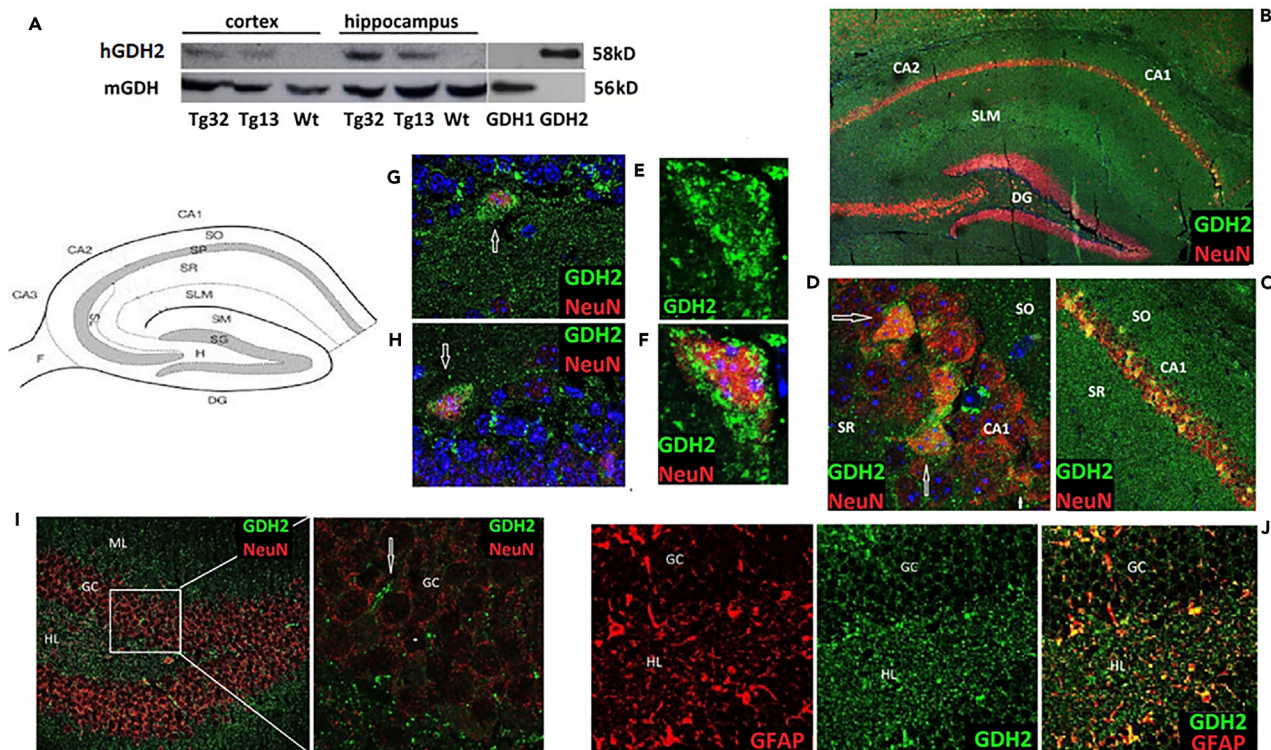


Figure 1. *GLUD2* expression in Tg mice brain

(A) Immunoblots of brain extracts from adult **Tg13**, **Tg32** and wild-type (**Wt**) mice probed with the anti-hGDH1 and anti-hGDH2 specific antibodies. Recombinant purified human GDH1 and human GDH2 are used as standards (**GDH1** and **GDH2**). A 58 kD hGDH2-specific band is detected in Tg mice only. On the other hand, Wt and Tg mice express the endogenous mGDH corresponding to the hGDH1 (56 kD band) at comparable levels.

(B) Double IF Images (x10) of hippocampus reveal a laminated-like pattern of hGDH2 expression (green), with SLM, SO and SR being prominently labeled. In the CA1 region, hGDH2 is expressed by NeuN-positive pyramidal cells (yellow in merged images).

(C) The CA1 region at x40.

(D) Punctate hGDH2 labeling of NeuN-positive CA1 neurons (empty arrows) and of the neuropil (x60).

(E and F) Large hGDH2-specific "puncta" (consistent with mitochondrial clusters) in the perikaryon of a large pyramidal neuron. (x120).

(G and H) hGDH2 expression in hilar mossy-like cells of DG. Blue staining: TOPRO-labelled cell nuclei (x60).

(I) hGDH2 expression in the neuropil of the GC layer, ML and hilus (HL) of DG. The granule cells lack hGDH2 (x40 left; x80 right).

(J) In DG, hGDH2 co-localizes with GFAP in astrocytic processes (x60).

to Wt animals at all current stimulation intensities tested ($F(1,13) = 15.2$, $p = 0.001$, repeated measures ANOVA) (Figures 2B and 2C). Also, the recorded spontaneous events are markedly increased (x4-5 fold) in Tg mice as compared to the Wt animals (t-test, $p = 0.02$) (Figures 2D and 2E). Paired-pulse ratio, obtained by recording two pulses at different frequencies (10–50 Hz), is significantly increased in Tg mice for 20 Hz (t-test, $p = 0.03$) and for 50 Hz (t-test, $p = 0.02$) (Figures 2F and S5). The potentiation of fEPSP (% baseline fEPSP peak) following theta-burst stimulation is substantially enhanced in Tg than in Wt mice ($F(1,13) = 11.6$, $p = 0.005$, repeated measures ANOVA) (Figure 2G).

*D-lactate blocks the *GLUD2*-induced late long-term potentiation enhancement*

Because increased neuronal activity stimulates the release of lactate by astrocytes and its uptake by neurons^{18,19} and because glutamate, metabolized in astrocytes via GDH-TCA cycle, is in part converted to lactate,^{20,21} we tested the effects of the inactive isomer D-lactate (capable of blocking the metabolism of L-lactate) in our hippocampal system. For this, we obtained theta-burst induced LTP in the absence or the presence of D-lactate and found that D-lactate essentially abolishes the enhanced late LTP phase (past 30min) in Tg animals (repeated measures ANOVA $F(1,11) = 5.6$, $p = 0.03$) (Figure 2I), while producing little effect in Wt mice (repeated measures ANOVA $F(1,8) = 3.5$, $p = 0.1$) (Figure 2H).

To further delineate the mechanisms of excitatory transmission that are altered in *GLUD2*, we performed patch-clamp recordings from CA1 pyramidal neurons and recorded sEPSCs at -70 mV, sIPSCs at $+10$ mV and sNMDACs at $+30$ mV following the application of bicuculline. Our results show that sEPSC amplitude is significantly increased while sEPSC frequency is not altered (Figure 3A). Regarding sIPSCs, we find no significant adaptations in either their amplitude or their frequency (Figure 3B). Finally, both the frequency and the amplitude of sNMDACs are significantly enhanced in *GLUD2* mice (Figure 3C).

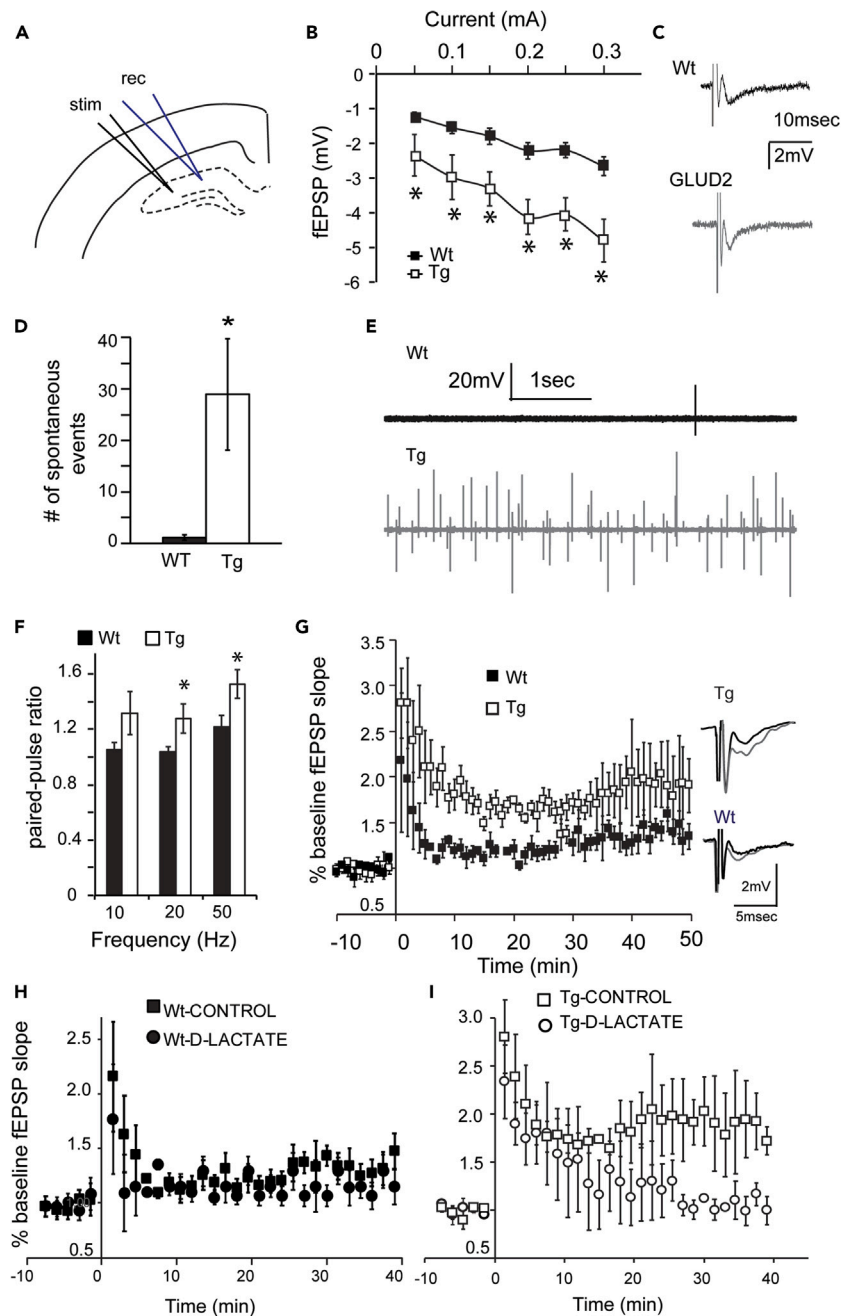


Figure 2. Enhanced hippocampal synaptic transmission and plasticity in Tg mice

Adult Tg mice (N = 7) and Wt (N = 7) animals were studied.

(A) Sites of stimulation and recording in the CA1 area of the cornu Ammonis.

(B) fEPSP recordings from the CA1 area following the stimulation of Schaffer collateral axons are significantly higher in Tg (*GLUD2*) mice than in Wt animals at all current stimulation intensities tested (* $F(1,13) = 15.2$, $p = 0.001$, repeated measures ANOVA).

(C) Representative traces showing enhanced fEPSPs in Tg mice.

(D) Spontaneous events in Wt and Tg mice (t-test, * $p = 0.02$).

(E) Representative traces of spontaneous activity from Wt and Tg mice.

(F) Paired-pulse ratio obtained by recording two pulses at 10, 20 and 50 Hz in Wt and Tg (*GLUD2*) mice (t-test, $p = 0.2$, * $p = 0.03$ and ** $p = 0.02$ respectively). (G) Graph (left) and representative traces (right) show enhanced fEPSP potentiation (% baseline fEPSP peak) following theta-burst stimulation in Tg mice ($F(1,13) = 11.6$, $p = 0.005$, repeated measures ANOVA).

(H and I) D-lactate (10 μM) markedly attenuates late LTP (30 min post theta burst potentiation) in Tg mice (reduction by 60%) (I) compared to Wt (H) animals (reduction by 20%). Control: LTP obtained in Tg or Wt mice without D-lactate. Dots and Columns represent average values and bars SEM.

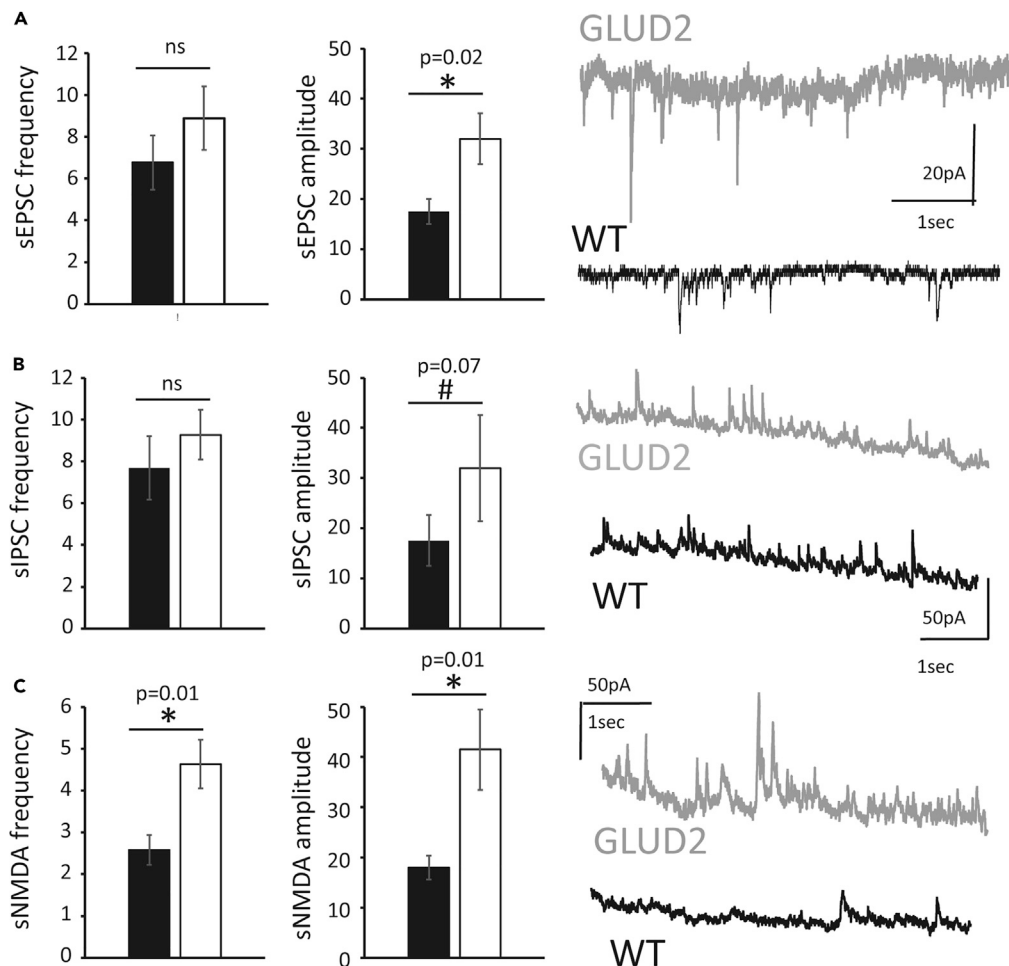


Figure 3. *GLUD2* enhances the sEPSC and sNMDA current amplitude

Adult *GLUD2* Tg mice (N = 8 cells; from 6 animals) and WT mice (N = 6 cells, 1 from each animal).

(A) Graphs (left) and representative traces (right) show that sEPSC frequency is not altered (t-test, $p = 0.31$) in *GLUD2* mice while sEPSC amplitude is significantly increased in *GLUD2* mice (t-test, $p = 0.02$).

(B) Graphs (left) and representative traces (right) showing that sIPSC frequency is not altered in *GLUD2* mice (t-test, $p = 0.45$) while there is a trend toward an increase in sIPSC amplitude in *GLUD2* mice (t-test, $p = 0.08$).

(C) Graphs (left) and representative traces (right) showing that sNMDA current frequency and sNMDA current amplitude are significantly increased in *GLUD2* mice (t-test, $p = 0.01$ for both frequency and amplitude).

Columns represent mean values and bars SEM.

Together, our data demonstrate that the Tg expression of this single human gene in hippocampal neurons and astrocytes markedly enhances excitatory transmission and plasticity, processes essential for cognitive functions. Indeed, our electrophysiology recordings in Tg hippocampus revealed significant enhancement of LTP, which is thought to represent the cellular correlate of long-term memory²² The enhanced synaptic plasticity observed in hippocampal synapses likely depends on the enhanced NMDA receptor function as this was observed in sNMDA current recordings. Moreover, D-lactate abrogates the *GLUD2*-induced augmentation of LTP, suggesting that the enhancement of synaptic plasticity by *GLUD2* transgenic expression depends, at least in part, on the lactate-mediated metabolic interaction between astrocytes and neurons.

GLUD2 enhances dendritic spine formation and synaptogenesis in the hippocampus

As these observations reveal that the transgenic expression of *GLUD2* is sufficient to potentiate glutamatergic transmission and synaptic plasticity, we then used the Golgi-Cox staining method to study the effect of this single gene on the density of hippocampal dendritic spines and on synaptogenesis. Results reveal that Tg animals exhibit a significantly increased density of dendritic spines (particularly of the mature spines) throughout their life span (Figure 4). In 15-day-old Tg mice, the mature dendritic spines are significantly increased as compared to the Wt mice of the same age, although the stubby spines are decreased (Figure 4C). On the other hand, 6-months-old Tg mice exhibit significant

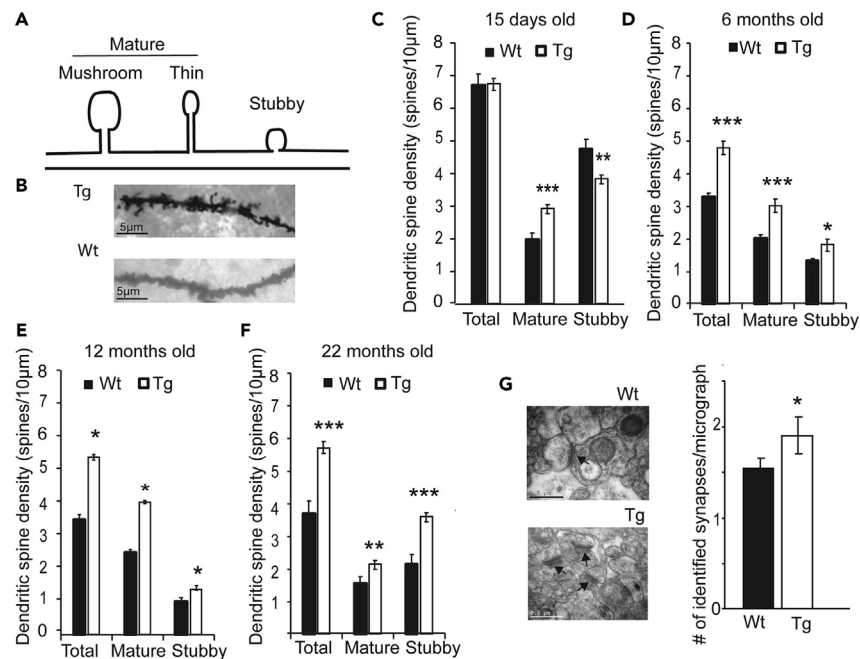


Figure 4. *GLUD2* Enhances Dendritic Spine Density and Synaptogenesis in Hippocampus

(A) Schematic representation of stubby and mature dendritic spines.

(B) Hippocampal dendritic spines in 6-month-old Wt and Tg mice revealed by the Golgi-Cox stain.

(C) At 15 days of age, the density (spines/10 µm) of mature dendritic spines is higher in Tg (N = 3) than in Wt (N = 3) mice (***p = 0.0004), whereas the density of stubby spines is decreased in Tg animals (**p = 0.01).

(D) At 6-month of age, Tg mice (N = 5) show increased density for total (***p = 0.0004), mature (***p = 0.0005) and stubby (*p = 0.02) dendritic spines, as compared to Wt mice (N = 5).

(E) At 12-month of age, Tg mice (N = 4), exhibit increased density for total (*p = 0.03), mature (*p = 0.02) and stubby (t-test, *p = 0.02) dendritic spines, as compared to Wt littermates (N = 4).

(F) Aged 22-month-old Tg mice (N = 3) show a greater density of total (***p = 0.0003), mature (**p = 0.002) and stubby (***p = 0.0001) spines than aged Wt (N = 3) animals.

(G) EM images of synapses in the hippocampus of a Tg mice (left bottom) as compared to a Wt mouse (left top). Synapses were counted in 79 micrographs from 3 Wt mice and in 98 micrographs from 3 Tg mice, yielding a total of 120 synapses for the Wt and 174 synapses for the Tg mice. The Graph shows that the average number of synapses per micrograph in Tg mice (N = 3) are greater than those in Wt mice (N = 3) (*p < 0.05). Columns are mean values and bars SEM. p values obtained by the t-test.

increases, compared to 6-month-old Wt animals, in the density of both the mature (t-test, $p = 0.0005$) and the stubby (t-test, $p = 0.02$) dendritic spines. As a result, the total dendritic spines are significantly increased (t-test, $p = 0.0004$) (Figure 4D). Also, at 12 months of age, Tg mice exhibit increased density for total (t-test, $p = 0.03$), mature (t-test, $p = 0.02$) and stubby (t-test, $p = 0.02$) dendritic spines as compared to 12-month-old Wt animals (Figure 4E). Similarly, aged Tg mice (22 months of age) show a greater density of total (t-test, $p = 0.0003$), mature (t-test, $p = 0.002$) and stubby (t-test, $p = 0.0001$) spines as compared to aged Wt animals (Figure 4F). The *GLUD2* effect on dendritic spine density is found in both of our Tg lines (Tg13 and Tg32) (Figure S6). To further test whether the increased dendritic spine density in Tg mice is associated with enhanced synaptogenesis, we studied the number and morphology of synapses in the hippocampus of adult, 6-month-old, Tg and Wt mice using Electron Microscopy (EM). Results reveal that the number of EM-identified synapses are significantly increased in the Tg mice as compared to their wild-type littermates (Figure 4G).

Together these data demonstrate that *GLUD2* promotes the formation of putative excitatory synapses and dendritic spines that are essential for new neuronal connections and represent the structural basis for long-term memory. The present data are congruent with previous observations showing that glutamate signaling is essential for the development and maintenance of dendritic spines^{23,24} Importantly, the increased hippocampal dendritic spine density is observed throughout the life span of the Tg animals, with a robust effect detected in aged (22-month-old) mice.

***GLUD2* enhances sensitivity to thermally induced pain and the innate rodent aversion to lighted and open spaces**

As these observations demonstrate that *GLUD2* potentiates functional and structural synaptic plasticity, processes involved in sensory functions, we evaluated the sensitivity of our Tg and Wt mice to sensory stimuli. In this context, we also studied the expression of *GLUD2* in the spinal cord, which plays a major role in the perception and modification of sensory input. Results of these morphological studies, performed

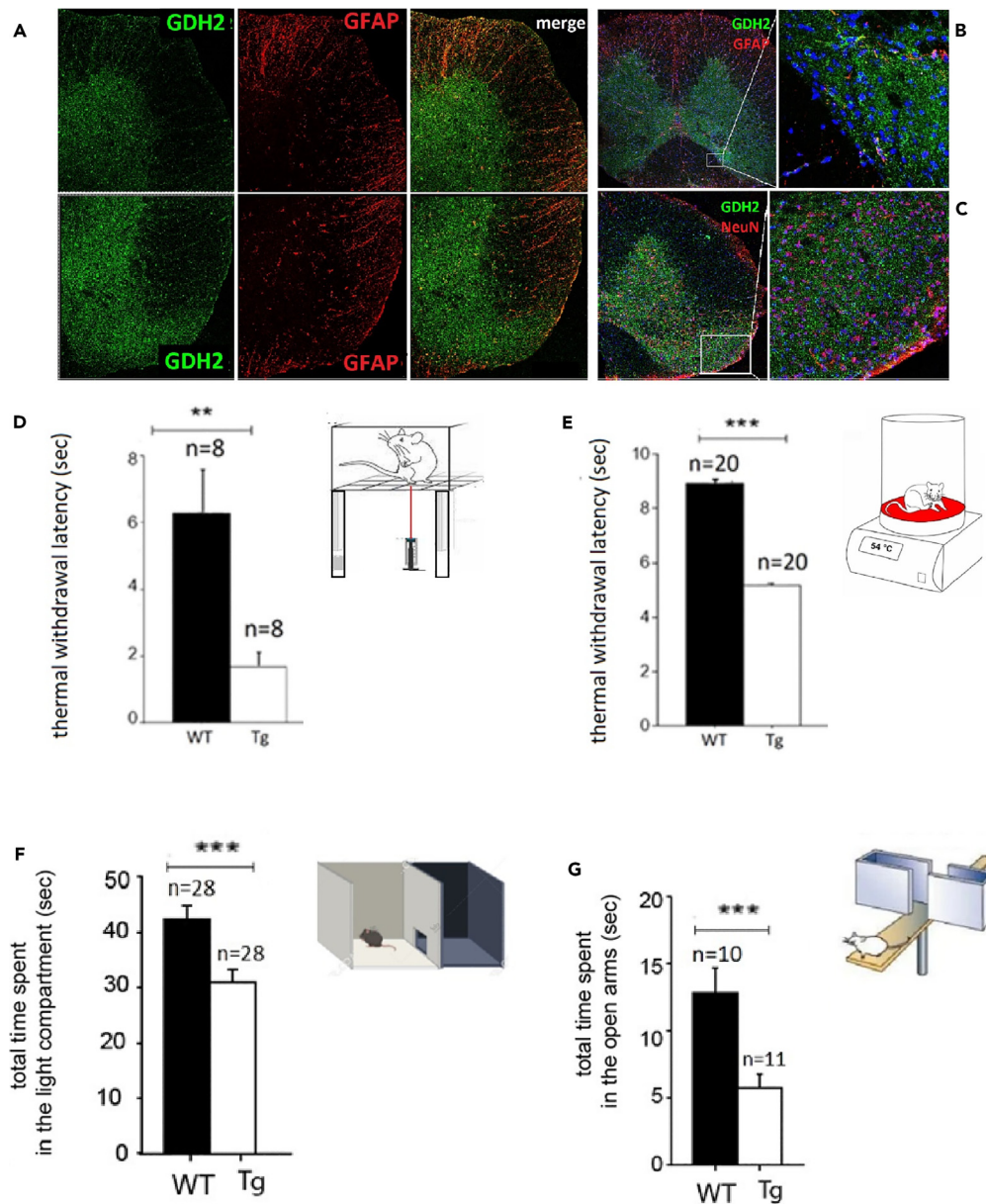


Figure 5. *GLUD2* expression enhances pain sensitivity and aversion to lighted and open spaces

(A–E) Double IF images of the spinal cord from a Tg13 (A) and Tg32 (B and C) mouse, reveals hGDH2 expression in the neuropil of the gray matter, with the dorsal horns being prominently labeled. (B) The dorsal horn expression is not associated with GFAP positive processes. (x80, x240). (C) NeuN-positive neurons lack hGDH2 in their perikaryon (x80, x240).

(D and E) Tg mice are more sensitive than Wt mice to thermally induced pain. Results, generated by the Hargreaves' method (** $p < 0.001$), are corroborated in D. and those obtained by the "Hot Plate" test (** $p < 0.0001$) in E.

(F and G) *GLUD2* enhances light and open space avoidance. (F) Light-Dark Test. The Tg mice remained in the lighted chamber significantly less time than the Wt animals (** $p = 0.001$). (G) The Elevated Plus Maze. The time spent in the open arm of the apparatus is significantly less for the Tg than for the Wt mice (** $p = 0.003$), indicating increased open space avoidance. Columns represent average values and bars SEM.

with the use of double IF-confocal microscopy, reveal the hGDH2-specific labeling of spinal cord gray matter, with the dorsal horn gray matter (an important sensory receptive area) being prominently labeled (Figures 5A and 5B). On the other hand, no hGDH2-specific labeling is found in GFAP positive processes within the neuropil of the spinal cord gray matter (Figures 5A–5C).

For testing the sensitivity of our animals to thermally induced pain, we employed two methods: the Hargreaves procedure that uses an infrared heat stimulus and the "Hot Plate" method. Results, obtained by the Hargreaves method, reveal that Tg mice are substantially

more sensitive to painful thermal stimuli than Wt animals (t-test, $p < 0.001$) (Figure 5D). This finding is corroborated by the “Hot Plate” test, which also shows that Tg mice are considerably more sensitive to thermally induced pain than the Wt mice (t-test, $p < 0.001$) (Figures 5D and 5E). The *GLUD2* effect on pain sensitivity is detected in both our Tg lines (Tg13 and Tg32) (Figure S7).

We then evaluated our Tg and Wt mice for their innate tendency to avoid environmental illumination and open spaces by using the Light/Dark Test and the Elevated Plus Maze test, respectively. We find that during the Light/Dark Test, the Tg mice spend significantly less time in the lighted than in the dark chamber as compared to their Wt littermates (Figure 5F). Similarly, during the Elevated Plus Maze test, the Tg mice remain in the open chamber of the apparatus for a significantly shorter amount of time than the Wt animals (Figure 5G). On the other hand, the spontaneous mobility of the Tg mice, recorded as the horizontal spontaneous activity, is similar between the Tg and the Wt mice (data not shown).

These data, demonstrating that *GLUD2* Tg expression enhances the animals’ sensitivity to painful stimuli, are congruent with previous observations showing that glutamate signaling plays an important role in pain perception and modification²⁵ and that enhanced glutamate-induced neuroplasticity leads to pain sensitization.²⁶ We also find here that *GLUD2* Tg expression potentiates the known aversion of rodents to environmental illumination and to open spaces. Such behavior has been correlated with increased anxiety²⁷ and linked to glutamatergic mechanisms²⁸ and dendritic spine density. There is even evidence that anxiety-like behavior is evolutionary advantageous, with genes sensitizing humans to anxiety being positively selected.²⁹

***GLUD2* expression improves attention set-shifting memory and contextual fear extinction, but not novel object recognition/location memory**

As our data reveal that *GLUD2* potentiates hippocampal excitatory transmission and synaptic plasticity along with metabolic processes involved in memory formation, we explored the possible effect of the human gene on cognitive functions. For this, we employed a battery of behavioral tasks that evaluate different cognitive functions, including attention set-shifting, contextual fear conditioning/extinction, novel object location, novel object recognition and right-left discrimination.

The Attentional Set-Shifting task (AS-ST) represents a measure of cognitive flexibility^{30,31} is tested by training mice to dig through the bowls under changing environmental conditions in order to get their reward. Seven phases are evaluated as described in the Legend of Figure 6 and in the STAR Methods. Results of the AST reveal that Tg mice performed significantly better than Wt mice on the compound discrimination reversal (CDR) phase ($p = 0.01$) (Figure 6A); they also showed a trend for improved performance on the simple discrimination (SD) phase ($p = 0.06$) and on the intradimensional reversal (IDR) phase ($p = 0.08$) (Figure 6A). On the other hand, Tg and Wt mice performed equally well on the compound discrimination (CD), intradimensional shift I and II (IDI&IDII) and the ES phases (Figure 6A).

During the Contextual Fear Conditioning/Extinction (CFC/E) task, Tg and Wt mice receive a single electric shock while in the conditioning chamber (context) (Figure 6B). Then, upon subsequent return to the context the mice are monitored daily for the characteristic fear behavior of freezing.³² Results of the CFC/E task reveal that Tg mice ($N = 12$) exhibit on day 5 of extinction training substantially less freezing than Wt mice ($N = 12$) (reduction by more than 50%; t test $p = 0.01$), a finding consistent with enhanced contextual fear extinction. However, on day 1 of training, Tg mice experience less freezing than Wt mice (reduction by about 20%, t-test $p = 0.04$) (Figure 6B) suggestive of decreased fear memory. To determine whether this affected the freezing of *GLUD2* animals on day 5, as found here, the values of % freezing for days 2,3,4 and 5 were normalized to the % freezing for day 1 for each animal. Statistical comparisons of the normalized data still reveal that *GLUD2* mice experience significantly less freezing on day 5 than Wt mice (t-test, $p = 0.03$) (Figure S8).

The Novel Object Recognition Task (Recognition Memory) is based on the inherent preference of mice for novelty. During the trial phase of the task, the animals are allowed to explore two identical objects (object 1 and 2) placed in the arena, whereas during the test phase, the animals are re-introduced in the arena, where one of the original objects had been replaced by a new object; the time spent by the mice to explore the novel object over that of the familiar object is considered recognition memory. Results reveal that, while during the trial phase the mice show no preference for object 1 or object 2 (Figure S9), during the test phase they spend significantly more time interacting with the novel object than with the familiar one (t-test, $p = 0.01$ for Wt mice and $p = 0.004$ for Tg *GLUD2* mice). The Wt mice and the Tg mice do not differ significantly regarding their estimated recognition memory, with the discrimination index being comparable for the two animal groups (Figure 6D).

Location memory was tested with the Object-to-Place Task. During the trial phase of this task, the mice are allowed to explore two objects (object 1 and 2) placed in the arena, whereas during its test phase, the animals are re-introduced in the arena, where one of the original objects had been moved to a novel location. Results reveal that, while the animals show no preference for object 1 or 2 during the trial phase (Figure S10), both Wt and Tg *GLUD2* mice spend more time interacting with the displaced (novel) object than with the stationary (familiar) object (t-test, $p = 0.0004$ for Wt mice; t-test, $p = 0.009$ for *GLUD2* mice). No significant differences are found in the discrimination index between the two experimental groups (Figure 6F). In addition, using the Left-Right Discrimination task to assess reference memory,³³ we find no significant differences between Tg and Wt mice although there is a trend for decreased performance of the Tg animals ($p = 0.07$, one way ANOVA) (Figure S11).

Together these observations reveal that *GLUD2* Tg expression enhances cognitive functions that are rather complex, such as aspects of behavioral flexibility (compound discrimination reversal of the attentional set-shifting task) and extinction of conditioned fear that represents a form of inhibitory learning.³² On the other hand, *GLUD2* Tg expression had no significant effects on the evolutionary conserved novel object recognition, novel object location memory and reference memory (left-right discrimination).

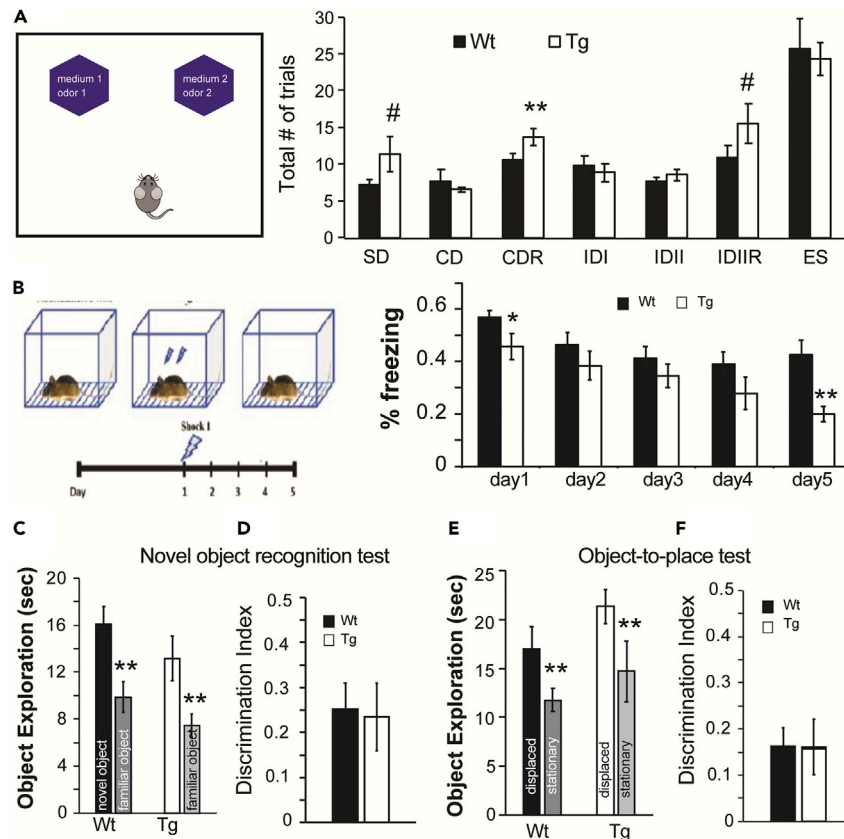


Figure 6. Effect of Tg *GLUD2* Expression on Attentional Set-Shifting Task (AS-ST), Contextual Fear Conditioning/Extinction (CFC/E) and Novel Object Recognition/Location Memory

(A) AS-ST: for simple discrimination (SD) mice need to discriminate between two different bedding materials (substrates) in order to get their reward; for compound discrimination (CD), two different odors are added as distractor stimuli; for compound discrimination reversal (CDR), the same substrates and odors are used, but the rewarding substrate is reversed; for intradimensional shift I (IDI), the pair of digging media (substrates) and odors are replaced with new ones; for intradimensional shift II (IDII), the substrates are replaced with new pair, one being the rewarded digging media; for intradimensional reversal, (IDR) the correct and the wrong digging media are reversed while the odors are replaced by a new pair; for extradimensional shift (EDS), the digging media and odors are replaced by new ones, but the reward is now governed by the odors. Tg (*GLUD2*) (N = 6) mice perform significantly better than Wt (N = 6) mice on the CDR phase (**p = 0.01) and also show a trend for improved performance on the SD (#p = 0.06) and the IDR phase (#p = 0.08). "total # of trials" to reach criterion (6 consecutive correct trials).

(B) CFC/E: Tg (N = 12) and Wt (N = 12) mice receive an electric shock while in the conditioning chamber and then monitored daily upon returning to the chamber (See STAR Methods). % freezing is the percentage of the time the animal displayed the characteristic freezing behavior while in the chamber (1.0 = 100%). (**p = 0.01; *p = 0.04).

(C and D) Novel object recognition test. Both Wt (N = 9) and Tg (*GLUD2*) (N = 10) mice spend significantly more time (in seconds) exploring the novel than the familiar object (Object Exploration) (**p = 0.01 for Wt; *p = 0.004 for Tg mice). The Discrimination Index is determined by the formula: $DI = (N - F) / (N + F)$ where N is the time spent for the novel and F for the familiar object.

(E and F) Object to place-test. Again, Wt and Tg (*GLUD2*) (N = 11) mice spend more time exploring the displaced than the stationary object (**p = 0.0004 for the Wt and *p = 0.009 for the *GLUD2*). Columns represent average values and bars SEM. Statistical analyses by the two-sample t-test and one-way ANOVA.

Discussion

The human *GLUD2* gene arose in the hominoid ancestor and evolved under positive Darwinian selection indicative of adaptive DNA sequence evolution. This equipped hGDH2 with unique functional properties that enable marked enzyme activation (through an ADP-dependent mechanism dissociated from GTP control) under intense neuronal firing and high energy utilization, processes required for synaptic plasticity and memory consolidation. As *GLUD2* evolved concomitantly with human brain expansion, the novel gene may have contributed to the rapid emergence of human cognitive abilities.^{10,12} To explore this possibility and better understand the potential role of the recently emerged evolved human gene in brain biology we investigated here the effect of *GLUD2* transgenic expression on structural, physiological and behavioral aspects of cognitive function.

Our morphological studies on *GLUD2* Tg hippocampus, using an antibody specific for hGDH2, reveals the specific expression of the human protein in pyramidal cells of the SP (CA1-CA3) and in the hilar mossy-like cells of the sub granular area of DG, hippocampal neurons are

crucial to memory processes. On the other hand, the numerous granule cells of the hippocampus are negative for hGDH2-specific immunoreactivity. We also find hGDH2 expression in astrocytes located in SO, SLM and SR, including the CA1 region of the SR where the synapses of CA3/CA1 pyramidal cells occur. These observations are largely consistent with the hGDH2 expression pattern detected both in human and Tg mouse cerebral cortex. Specifically, the study of multiple regions of human frontal, parietal and temporal lobe (derived from 10 non-neurologic subjects)¹⁶ and that of multiple coronal sections of Tg mouse brain¹² revealed a uniform expression pattern that includes hGDH2 expression in astrocytes and in cortical neurons with pyramidal morphology, but not in other types of cortical neurons. As such, our present morphological observations provide additional evidence that our Tg animal model can be usefully employed for studying the role of *GLUD2* in brain biology.¹²

Electrophysiological studies on hippocampal slices obtained from Tg and Wt mice reveal that the human gene enhances theta-burst induced LTP in CA3-CA1 synapses and that these responses are markedly attenuated by D-lactate, indicating that L-lactate metabolism is essential to these processes. Patch clamp experiments further reveal that the amplitude of sEPSC is significantly increased in hippocampal synapses of the Tg mice as compared to the Wt animals, although the sEPSC frequency, an indicator of presynaptic activity, is not significantly altered. These observations argue against the possibility that *GLUD2* enhances glutamatergic transmission by increasing presynaptic glutamate release. Instead, our findings showing that *GLUD2* enhances both the frequency and the amplitude of sNMDA currents, support the view that the human gene potentiates LTP by enhancing NMDA receptor signaling. Also, our observations, showing that blocking the metabolism of L-lactate by D-lactate aborts the effect of *GLUD2* on LTP, are consistent with this possibility, given that L-lactate positively modulates NMDA receptor activity.^{34,35}

Our data, demonstrating that *GLUD2* enhances synaptic plasticity (LTP) through a lactate-dependent mechanism, rather than glutamate release, are congruent with the metabolomic and transcriptomic analyses of *GLUD2* Tg mice by Li et al.,³⁶ revealing that lactate levels were consistently elevated in the cerebral cortex of the Tg mice over their lifespan, whereas cerebral glutamate concentrations were normal. The mice studied by Li et al.³⁶ are transgenic for the same human genomic region that contains the *GLUD2* gene (RP11-610G22) as our Tg animals are. Li et al.³⁶ also found that *GLUD2* upregulates the "carbon metabolism" pathway, including the TCA cycle and its linked HIF-1 signaling pathway, and the pentose-phosphate pathway. Nissen et al.¹⁵ subsequently studied Tg brain astrocytes from the same Tg mice, expressing both the human hGDH2 and the endogenous rodent GDH1 and found that Tg astrocytes exhibit enhanced capacity to take up and metabolize glutamate through the TCA cycle. Importantly, the *GLUD2* effect was seen only when astrocytes were exposed to relatively high glutamate concentrations (0.5 mM), but not when conventional concentrations of glutamate (0.1–0.25 mM) were used.¹⁵ These results accord our model that hGDH2 is activated by intense glutamatergic firing and consequently by high synaptic glutamate concentrations (expected to reach >1.0 mM).

By augmenting the capacity of glutamate uptake and of the TCA cycle, *GLUD2* enhances the ability of synaptic astrocytes to clear up this potentially toxic amino acid from the synaptic cleft and to boost their energy stores particularly upon intense neuronal firing, a high energy-demanding process. Because GDH is essential for glutamate-fueled respiration upon excitation³⁷ and because mitochondrial respiration generates ROS,³⁸ upregulation of the pentose-phosphate pathway by *GLUD2* may protect against oxidative stress associated with intense excitatory transmission. Moreover, the effect of *GLUD2* on the TCA cycle-linked HF-1 signaling pathway, as noted above, may provide another mechanism for L-lactate production through glycolysis,³⁹ which may operate in parallel with the glycogenolysis pathway that is stimulated by neuronal activity and that is crucial for cognitive processes as shown by Suzuki et al.⁴⁰

The present observation that hGDH2 is densely expressed in hippocampal pyramidal cells raise important questions regarding the role of the newly evolved human enzyme in the biology of these neurons, characterized by their intense energy-demanding excitatory activity. Our findings suggesting that glutamate release is not increased in Tg mouse hippocampus, make it unlikely that *GLUD2* potentiates glutamatergic activity and plasticity by enhancing presynaptic glutamate production. Instead, the enzyme may enhance neuronal glutamate catabolism and energy production, as suggested by previous metabolic investigations.³⁷ Indeed, studies on isolated nerve terminals and cultured glutamatergic neurons revealed that GDH function augments the capacity of the TCA cycle to oxidize acetyl-CoA formed from glucose, with this pathway being essential for increasing glutamate-fueled respiration when elevated energy demands (intense excitatory transmission) prevail.³⁷ Hence, by boosting the energy status of neurons during the high energy-demanding cognitive processes, *GLUD2* may have provided a biological advantage that contributed to the evolution of traits unique to humans.

We also demonstrate here that *GLUD2*-enhanced glutamate signaling increases the density of dendritic spines and synaptogenesis in the hippocampus. Specifically, our study reveals that the mature spines are significantly increased in Tg mice throughout their lifespan, whereas stubby spines are increased during adulthood and aging. The mature spines include the thin and the mushroom spines, while the stubby spines are considered immature. The thin spines are known to exhibit a high degree of plasticity, being able to evolve into mushroom spines in response to synaptic signaling.⁴¹ The thin spines are considered by some as "learning spines," whereas the more stable mushroom spines as "memory spines."^{41,42} Both types of mature spines are thought to predominate during adult life, whereas stubby spines are prevalent during early post-natal development.⁴¹ Our findings on control (Wt) animals accord these considerations by showing that the density of the stubby spine in 15-day-old Wt mice is 2.5-fold greater than that of the mature spines, whereas in adult Wt mice the mature spines predominate. However, in aged (22 months old) Wt mice we find that the density of mature spines is decreased and that of stubby spines is increased. Similar findings have also been described in old mice by Aguilar-Hernandez et al.,⁴³ who attributed these changes to the aging process.

Our data demonstrate that *GLUD2* enhances LTP in CA1 synapses leading to increased spinogenesis/synaptogenesis in the hippocampus, accord previous observations⁴⁴ showing that LTP promotes the formation of new synapses in postsynaptic dendrites in hippocampal CA1 neurons. Conversely, lesioning of Schaffer collaterals leads to decreased spine density.⁴² Activity-dependent regulation of synapses requires

the activation of the NMDA receptors in the hippocampus,⁵ a process enhanced by *GLUD2* transgenic expression as our data show. The NMDA receptors are the predominant source of synaptically evoked Ca^{2+} that regulates several processes, including functional and structural synaptic plasticity.⁴⁵ The trophic effect of *GLUD2* on mature dendritic spines during post-natal brain development may also be linked to the ability of the human gene to upregulate the expression of several genes involved in neurogenesis, neuronal differentiation and maturation.³⁶ Given that most excitatory synapses in the CNS are formed in dendritic spines⁴¹ and that activity-dependent synaptic connections are central to learning and memory,⁴⁶ our findings suggest that the strengthening of glutamatergic transmission by *GLUD2* evolution enhances the inter-neuronal connectivity network that underlies human cognitive abilities.

Compared to that of other primates, the human brain has a higher density of dendritic spines and synaptic connections.⁴⁶ This elevated dendritic spine density has been linked to the high synaptic activity that characterizes the human brain¹ with the new synaptic contacts between neurons providing a substrate for learning and memory.⁴⁶ Hence, our data demonstrating that synaptic activity and spinogenesis are enhanced in Tg mice, suggest that the expression of the human hGDH2 protein in Tg mice recapitulates aspects of physiological and morphological characteristics of human brain.

Regarding the effect of *GLUD2* on behavior, our data demonstrate that Tg mice exhibit improved performance on aspects of the AS-S task, which evaluates behavioral flexibility in response to changing external demands, thus representing a measure of behavioral adaptation.³⁰ Specifically, AS-ST tests the ability of mice to learn simple rules and to modify their response when the rules have changed. Because this involves the inhibition of a previously acquired strategy and learning of a new one, behavioral flexibility is considered a form of higher cognitive function.⁴⁷ In addition, we find that *GLUD2* enhances contextual fear conditioning/extinction that assesses the formation and retrieval of new memories required for the extinction process and that depends on glutamatergic transmission.³² On the other hand, *GLUD2* had no significant effects on the evolutionary conserved novel object recognition, novel object location and reference memory (left-right discrimination).

Because the behavioral outcomes of enhanced plasticity may depend on the animal's recent history of activities⁴⁸ and because *GLUD2* enhances synaptic plasticity evoked by stimulation, the novel human gene may promote experience-dependent learning and memory. As human brain exhibits a greater degree of cerebral cortical plasticity than chimpanzee brain,⁴⁹ environmental influences may play a prominent role in shaping human cognitive advancement, particularly during early brain maturation, at which stage the *GLUD2* gene is maximally active.³⁶

Congruent with these possibilities are findings on human newborns demonstrating higher levels of the expression of *GLUD2* and lower glutamate contents (indicative of an increased turnover) as compared to chimpanzee newborns.¹ Our work, providing evidence that *GLUD2* may have contributed to human brain evolution by enhancing lactate-mediated astrocyte-neuron interaction, is in accordance with recent high-throughput single-cell comparative transcriptomic analyses of human-specific cortical features,⁵⁰ revealing that genes exhibiting cell specific expression changes, are particularly in pathways linked to neuronal and glial communication.⁵⁰

Importantly, our findings, demonstrate that *GLUD2*-enhanced glutamate signaling promotes the formation of new synaptic connections and that this process is active throughout the lifespan of the animals, extending to 22 months of age. As previous studies on human brain have shown that a high density of dendritic spines protects from age-related degeneration,⁵¹ these observations, taken together, raise the possibility that the genetic enhancement of structural plasticity via *GLUD2* may protect human brain from senescence, perhaps contributing to increased longevity of the humans as compared to other primates.

Limitations of study

As it is generally acknowledged, conclusions deriving from the rodent model to human physiologic mechanisms should be accepted with caution. The possibility that our findings relate to alterations of the mouse genome induced by the random (stochastic) insertion of the human DNA, has been excluded by obtaining essentially identical results on two transgenic lines (Tg13 and Tg32) constructed independently. The possibility of the aberrant expression of the human protein in the host mouse brain, at times encountered when non-natural promoters are used, is highly unlikely here as our Tg mice were constructed using a segment of the human X chromosome containing the *GLUD2* gene and its natural regulatory elements. Indeed, the cellular and subcellular distribution of hGDH2 in the host mouse brain, is essentially identical to that previously observed in human brain. Whereas the present study explored the effect of *GLUD2* on structural and physiologic characteristics of the hippocampus, the observed behavioral findings likely relate to the putative expression of the human protein in other brain regions of the host (including the prefrontal cortex) involved in the behaviors tested. Lastly, another limitation of our study is the fact that all of our Wt and Tg mice are males. Hence, it cannot be ascertained whether the gender of the animals could have affected our findings. Obviously, more extensive studies are needed to address important issues raised by the present investigations.

STAR★METHODS

Detailed methods are provided in the online version of this paper and include the following:

- KEY RESOURCES TABLE
- RESOURCE AVAILABILITY
 - Lead contact
 - Materials availability
 - Data and code availability
- EXPERIMENTAL MODEL AND STUDY PARTICIPANT DETAILS

- Ethical statement for animal experiments
- Experimental animals
- **METHOD DETAILS**
 - Western blots of brain tissue
 - Brain slice preparation
 - Double immunofluorescence staining
 - Golgi-Cox staining
 - Electron microscopy
 - Electrophysiology
 - Behavioral experiments
- **QUANTIFICATION AND STATISTICAL ANALYSIS**
 - Brain morphological analysis
 - Electrophysiological studies analysis
 - Behavioral experiments analyses

SUPPLEMENTAL INFORMATION

Supplemental information can be found online at <https://doi.org/10.1016/j.isci.2024.108821>.

ACKNOWLEDGMENTS

AP and CS are supported by the European Union and the Operational Program “Education and Lifelong Learning” of the National Strategic Reference Framework (NSRF) - Research Funding Program: THALIS-UOA, Title “Mechanisms of pathogenesis of Parkinson’s disease” (Grant Code 70/3/11679). Special Account for Research Funds of the University of Crete- Research Funding Program Code Number:4379: “Studies on the molecular basis of neurodegenerative disorders”. This project has received funding from the European Union’s Horizon 2020 research and innovation program under the Marie Skłodowska-Curie grant agreement No 101007926. Title: Network analysis in neocortex during passive and active learning (CS and KS) and from the European Union’s Horizon Europe program *CHAngeing – Connected Hubs in Ageing: Healthy Living to Protect Cerebrovascular Function* (Excellence Hubs - HORIZON-WIDERA-2022-ACCESS-04-01) under grant agreement No. 101087071 (CS). The authors thank Irene Skoula for her technical support and Andreas Kastellakis for his help in horizontal locomotion behavioral studies. We are also grateful to George Chalepakis and the Electron Microscopy Facility “Vasilis Galanopoulos” for help with electron microscopy.

AUTHOR CONTRIBUTIONS

A.P., C.S. and K.S. designed and planned the study. C.S. designed, performed and evaluated the IF investigations (IF and so forth). K.S. designed, performed and analyzed the neural recordings, the dendritic spine density and the synapse quantitation. K.S. and C.S. designed the behavioral tasks. A.P., C.S., and K.S. wrote and edited the article. Z.P, K.D., K.M., X.K., and E.V. performed experiments on behavior (ZP and KD), morphology (ZP), and electrophysiology (XK, EV and KD). Visualization: CS, KS, ZP, KM, and KD.

DECLARATION OF INTERESTS

The authors declare no competing interests.

Received: November 11, 2022

Revised: October 18, 2023

Accepted: January 3, 2024

Published: January 19, 2024

REFERENCES

1. Fu, X., Giallisco, P., Liu, X., Catchpole, G., Fu, N., Ning, Z.-B., Guo, S., Yan, Z., Somel, M., Pääbo, S., et al. (2011). Rapid metabolic evolution in human prefrontal cortex. *Proc. Natl. Acad. Sci. USA* *108*, 6181–6186. <https://doi.org/10.1073/pnas.1019164108>.
2. Cáceres, M., Lachuer, J., Zapala, M.A., Redmond, J.C., Kudo, L., Geschwind, D.H., Lockhart, D.J., Preuss, T.M., and Barlow, C. (2003). Elevated gene expression levels distinguish human from non-human primate brains. *Proc. Natl. Acad. Sci. USA* *100*, 13030–13035. <https://doi.org/10.1073/pnas.2135499100>.
3. Muntané, G., Horvath, J.E., Hof, P.R., Ely, J.J., Hopkins, W.D., Raghanti, M.A., Lewandowski, A.H., Wray, G.A., and Sherwood, C.C. (2015). Analysis of synaptic gene expression in the neocortex of primates reveals evolutionary changes in glutamatergic neurotransmission. *Cerebr. Cortex* *25*, 1596–1607. <https://doi.org/10.1093/cercor/bht354>.
4. Rothman, D.L., Behar, K.L., Hyder, F., and Shulman, R.G. (2003). In vivo NMR studies of the glutamate neurotransmitter flux and neuroenergetics: Implications for Brain Function. *Annu. Rev. Physiol.* *65*, 401–427. <https://doi.org/10.1146/annurev.physiol.65.092101.142131>.
5. Malenka, R.C., and Nicoll, R.A. (1993). NMDA-receptor-dependent synaptic plasticity: multiple forms and mechanisms. *Trends Neurosci.* *16*, 521–527.
6. Prabhakar, S., Noonan, J.P., Pääbo, S., and Rubin, E.M. (2006). Accelerated Evolution of Conserved Noncoding Sequences in Humans. *Science* *314*, 786. <https://doi.org/10.1126/science.1130738>.
7. Cotney, J., Leng, J., Yin, J., Reilly, S.K., DeMare, L.E., Emera, D., Ayoub, A.E., Rakic, P., and Noonan, J.P. (2013). The Evolution of

- Lineage-Specific Regulatory Activities in the Human Embryonic Limb. *Cell* 154, 185–196. <https://doi.org/10.1016/j.cell.2013.05.056>.
8. Kronenberg, Z.N., Fiddes, I.T., Gordon, D., Murali, S., Cantsilieris, S., Meyerson, O.S., Underwood, J.G., Nelson, B.J., Chaisson, M.J.P., Dougherty, M.L., et al. (2018). High-resolution comparative analysis of great ape genomes. *Science* 360, eaar6343. <https://doi.org/10.1126/science.aar6343>.
 9. Shashidharan, P., Michaelidis, T.M., Robakis, N.K., Kresovali, A., Papamatheakis, J., and Plaitakis, A. (1994). Novel human glutamate dehydrogenase expressed in neural and testicular tissues and encoded by an X-linked intronless gene. *J. Biol. Chem.* 269, 16971–16976. [https://doi.org/10.1016/s0021-9258\(19\)89484-x](https://doi.org/10.1016/s0021-9258(19)89484-x).
 10. Burki, F., and Kaessmann, H. (2004). Birth and adaptive evolution of a hominoid gene that supports high neurotransmitter flux. *Nat. Genet.* 36, 1061–1063. <https://doi.org/10.1038/ng1431>.
 11. Plaitakis, A., Kalef-Ezra, E., Kotzamani, D., Zaganas, I., and Spanaki, C. (2017). The Glutamate Dehydrogenase Pathway and Its Roles in Cell and Tissue Biology in Health and Disease. *Biology* 6, 11. <https://doi.org/10.3390/biology6010011>.
 12. Plaitakis, A., Kotzamani, D., Petraki, Z., Delidakis, M., Rintotas, V., Zaganas, I., Douni, E., Sidiropoulou, K., and Spanaki, C. (2019). Transgenic Mice Carrying *GLUD2* as a Tool for Studying the Expressional and the Functional Adaptation of this Positive Selected Gene in Human Brain Evolution. *Neurochem. Res.* 44, 154–169. <https://doi.org/10.1007/s11064-018-2546-3>.
 13. Kanavouras, K., Mastorodemos, V., Borompokas, N., Spanaki, C., and Plaitakis, A. (2007). Properties and molecular evolution of human *GLUD2* (neural and testicular tissue-specific) glutamate dehydrogenase. *J. Neurosci. Res.* 85, 1101–1109. <https://doi.org/10.1002/jnr.21197>.
 14. Shashidharan, P., Clarke, D.D., Ahmed, N., Moschonas, N., and Plaitakis, A. (1997). Nerve Tissue-Specific Human Glutamate Dehydrogenase that Is Thermolabile and Highly Regulated by ADP. *J. Neurochem.* 68, 1804–1811. <https://doi.org/10.1046/j.1471-4159.1997.68051804.x>.
 15. Nissen, J.D., Lykke, K., Bryk, J., Stridh, M.H., Zaganas, I., Skyyt, D.M., Schousboe, A., Bak, L.K., Enard, W., Pääbo, S., and Waagepetersen, H.S. (2017). Expression of the human isoform of glutamate dehydrogenase, hGDH2, augments TCA cycle capacity and oxidative metabolism of glutamate during glucose deprivation in astrocytes. *Glia* 65, 474–488. <https://doi.org/10.1002/glia.23105>.
 16. Spanaki, C., Kotzamani, D., Kleopa, K., and Plaitakis, A. (2016). Evolution of *GLUD2* Glutamate Dehydrogenase Allows Expression in Human Cortical Neurons. *Mol. Neurobiol.* 53, 5140–5148. <https://doi.org/10.1007/s12035-015-9429-2>.
 17. Galakhova, A.A., Hunt, S., Wilbers, R., Heyer, D.B., de Kock, C.P.J., Mansvelter, H.D., and Goriounova, N.A. (2022). Evolution of cortical neurons supporting human cognition. *Trends Cognit. Sci.* 26, 909–922. <https://doi.org/10.1016/j.tics.2022.08.012>.
 18. Fray, A.E., Forsyth, R.J., Boutelle, M.G., and Fillenz, M. (1996). The mechanisms controlling physiologically stimulated changes in rat brain glucose and lactate: a microdialysis study. *J. Physiol.* 496, 49–57. <https://doi.org/10.1113/jphysiol.1996.sp021664>.
 19. Magistretti, P.J., and Allaman, I. (2018). Lactate in the brain: from metabolic end-product to signalling molecule. *Nat. Rev. Neurosci.* 19, 235–249. <https://doi.org/10.1038/nrn.2018.19>.
 20. Sonnewald, U., Westergaard, N., Petersen, S.B., Unsgård, G., and Schousboe, A. (1993). Metabolism of [¹³C]Glutamate in Astrocytes Studied by ¹³C NMR Spectroscopy: Incorporation of More Label into Lactate than into Glutamine Demonstrates the Importance of the Tricarboxylic Acid Cycle. *J. Neurochem.* 61, 1179–1182. <https://doi.org/10.1111/j.1471-4159.1993.tb03641.x>.
 21. McKenna, M.C. (2013). Glutamate Pays Its Own Way in Astrocytes. *Front. Endocrinol.* 4, 191. <https://doi.org/10.3389/fendo.2013.00191>.
 22. Lynch, M.A. (2004). Long-Term Potentiation and Memory. *Physiol. Rev.* 84, 87–136. <https://doi.org/10.1152/physrev.00014.2003>.
 23. Bhatt, D.H., Zhang, S., and Gan, W.-B. (2009). Dendritic Spine Dynamics. *Physiology* 71, 261–282. <https://doi.org/10.1146/annurev.physiol.010908.163140>.
 24. Kwon, H.-B., and Sabatini, B.L. (2011). Glutamate induces de novo growth of functional spines in developing cortex. *Nature* 474, 100–104. <https://doi.org/10.1038/nature09986>.
 25. Wozniak, K.M., Rojas, C., Wu, Y., and Slusher, B.S. (2012). The Role of Glutamate Signaling in Pain Processes and its Regulation by GCP II Inhibition. *Curr. Med. Chem.* 19, 1323–1334. <https://doi.org/10.2174/092986712799462630>.
 26. Isaev, D., Gerber, G., Park, S.K., Chung, J.M., and Randik, M. (2000). Facilitation of NMDA-induced currents and Ca²⁺ transients in the rat substantia gelatinosa neurons after ligand of L5–L6 spinal nerves. *Neuroreport* 11, 4055–4061. <https://doi.org/10.1097/00001756-200012180-00030>.
 27. Calhoun, G.G., and Tye, K.M. (2015). Resolving the neural circuits of anxiety. *Nat. Neurosci.* 18, 1394–1404. <https://doi.org/10.1038/nn.4101>.
 28. Masneuf, S., Lowery-Gionta, E., Colacicco, G., Pleil, K.E., Li, C., Crowley, N., Flynn, S., Holmes, A., and Kash, T. (2014). Glutamatergic mechanisms associated with stress-induced amygdala excitability and anxiety-related behavior. *Neuropharmacology* 85, 190–197. <https://doi.org/10.1016/j.neuropharm.2014.04.015>.
 29. Cagliani, R., Fumagalli, M., Pozzoli, U., Riva, S., Cereda, M., Comi, G.P., Pattini, L., Bresolin, N., and Sironi, M. (2009). A complex selection signature at the human AVPR1B gene. *BMC Evol. Biol.* 9, 123. <https://doi.org/10.1186/1471-2148-9-123>.
 30. Bissonette, G.B., Powell, E.M., and Roesch, M.R. (2013). Neural structures underlying set-shifting: Roles of medial prefrontal cortex and anterior cingulate cortex. *Behav. Brain Res.* 250, 91–101. <https://doi.org/10.1016/j.bbr.2013.04.037>.
 31. Heisler, J.M., Morales, J., Donegan, J.J., Jett, J.D., Redus, L., and O'Connor, J.C. (2015). The Attentional Set Shifting Task: A Measure of Cognitive Flexibility in Mice. *J. Vis. Exp.* 51944–51946. <https://doi.org/10.3791/51944>.
 32. Garelick, M.G., and Storm, D.R. (2005). The relationship between memory retrieval and memory extinction. *Proc. Natl. Acad. Sci. USA* 102, 9091–9092. <https://doi.org/10.1073/pnas.0504017102>.
 33. Shoji, H., Hagihara, H., Takao, K., Hattori, S., and Miyakawa, T. (2012). T-maze Forced Alternation and Left-right Discrimination Tasks for Assessing Working and Reference Memory in Mice. *J. Vis. Exp.* (60), 3300. <https://doi.org/10.3791/3300>.
 34. Jourdain, P., Rothenfusser, K., Ben-Adiba, C., Allaman, I., Marquet, P., and Magistretti, P.J. (2018). Dual action of L-Lactate on the activity of NR2B-containing NMDA receptors: from potentiation to neuroprotection. *Sci. Rep.* 8, 13472. <https://doi.org/10.1038/s41598-018-31534-y>.
 35. Yang, L., Yang, Q., Zhang, K., Li, Y.-J., Wu, Y.-M., Liu, S.-B., Zheng, L.-H., and Zhao, M.-G. (2014). Neuroprotective Effects of Daphnetin against NMDA Receptor-Mediated Excitotoxicity. *Molecules* 19, 14542–14555. <https://doi.org/10.3390/molecules190914542>.
 36. Li, Q., Guo, S., Jiang, X., Bryk, J., Naumann, R., Enard, W., Tomita, M., Sugimoto, M., Khaitovich, P., and Pääbo, S. (2016). Mice carrying a human *GLUD2* gene recapitulate aspects of human transcriptome and metabolome development. *Proc. Natl. Acad. Sci. USA* 113, 5358–5363. <https://doi.org/10.1073/pnas.1519261113>.
 37. Hohnholt, M.C., Andersen, V.H., Andersen, J.V., Christensen, S.K., Karaca, M., Maechler, P., and Waagepetersen, H.S. (2018). Glutamate dehydrogenase is essential to sustain neuronal oxidative energy metabolism during stimulation. *J. Cerebr. Blood Flow Metabol.* 38, 1754–1768. <https://doi.org/10.1177/0271678x17714680>.
 38. Murphy, M.P. (2009). How mitochondria produce reactive oxygen species. *Biochem. J.* 417, 1–13. <https://doi.org/10.1042/bj20081386>.
 39. Lum, J.J., Bui, T., Gruber, M., Gordan, J.D., DeBerardinis, R.J., Covello, K.L., Simon, M.C., and Thompson, C.B. (2007). The transcription factor HIF-1 α plays a critical role in the growth factor-dependent regulation of both aerobic and anaerobic glycolysis. *Genes Dev.* 21, 1037–1049. <https://doi.org/10.1101/gad.1529107>.
 40. Suzuki, A., Stern, S.A., Bozdagi, O., Huntley, G.W., Walker, R.H., Magistretti, P.J., and Alberini, C.M. (2011). Astrocyte-Neuron Lactate Transport Is Required for Long-Term Memory Formation. *Cell* 144, 810–823. <https://doi.org/10.1016/j.cell.2011.02.018>.
 41. Helm, M.S., Dankovich, T.M., Mandad, S., Rammer, B., Jähne, S., Salimi, V., Koerbs, C., Leibbrandt, R., Urlaub, H., Schikorski, T., and Rizzoli, S.O. (2021). A large-scale nanoscopy and biochemistry analysis of postsynaptic dendritic spines. *Nat. Neurosci.* 24, 1151–1162. <https://doi.org/10.1038/s41593-021-00874-w>.
 42. McKinney, R.A. (2010). Excitatory amino acid involvement in dendritic spine formation, maintenance and remodelling. *J. Physiol.* 588, 107–116. <https://doi.org/10.1113/jphysiol.2009.178905>.
 43. Aguilar-Hernández, L., Vázquez-Hernández, A.J., de-Lima-Mar, D.F., Vázquez-Roque, R.A., Tendilla-Beltrán, H., and Flores, G. (2020). Memory and dendritic spines loss, and dynamic dendritic spines changes are age-dependent in the rat. *J. Chem. Neuroanat.* 110, 101858. <https://doi.org/10.1016/j.jchemneu.2020.101858>.
 44. Engert, F., and Bonhoeffer, T. (1999). Dendritic spine changes associated with

- hippocampal long-term synaptic plasticity. *Nature* 399, 66–70. <https://doi.org/10.1038/19978>.
45. Runge, K., Cardoso, C., and de Chevigny, A. (2020). Dendritic Spine Plasticity: Function and Mechanisms. *Front. Synaptic Neurosci.* 12, 36. <https://doi.org/10.3389/fnsyn.2020.00036>.
 46. Rochefort, N.L., and Konnerth, A. (2012). Dendritic spines: from structure to in vivo function. *EMBO Rep.* 13, 699–708. <https://doi.org/10.1038/embor.2012.102>.
 47. Ragozzino, M.E. (2007). The Contribution of the Medial Prefrontal Cortex, Orbitofrontal Cortex, and Dorsomedial Striatum to Behavioral Flexibility. *Ann. N. Y. Acad. Sci.* 1121, 355–375. <https://doi.org/10.1196/annals.1401.013>.
 48. Nguyen-Vu, T.B., Zhao, G.Q., Lahiri, S., Kimpo, R.R., Lee, H., Ganguli, S., Shatz, C.J., and Raymond, J.L. (2017). A saturation hypothesis to explain both enhanced and impaired learning with enhanced plasticity. *Elife* 6, e20147. <https://doi.org/10.7554/elife.20147>.
 49. Gómez-Robles, A., Hopkins, W.D., Schapiro, S.J., and Sherwood, C.C. (2015). Relaxed genetic control of cortical organization in human brains compared with chimpanzees. *Proc. Natl. Acad. Sci. USA* 112, 14799–14804. <https://doi.org/10.1073/pnas.1512646112>.
 50. Boros, B.D., Greathouse, K.M., Gentry, E.G., Curtis, K.A., Birchall, E.L., Gearing, M., and Herskowitz, J.H. (2017). Dendritic spines provide cognitive resilience against Alzheimer's disease. *Ann. Neurol.* 82, 602–614. <https://doi.org/10.1002/ana.25049>.
 51. Jorstad, N.L., Song, J.H.T., Exposito-Alonso, D., Suresh, H., Castro-Pacheco, N., Krienen, F.M., Yanny, A.M., Close, J., Gelfand, E., Long, B., et al. (2023). Comparative transcriptomics reveals human-specific cortical features. *Science* 382, eade9516.
 52. Stavroulaki, V., Ioakeimidis, V., Konstantoudaki, X., and Sidiropoulou, K. (2021). Enhanced synaptic properties of the prefrontal cortex and hippocampus after learning a spatial working memory task in adult male mice. *J. Neurosci. Res.* <https://doi.org/10.1002/jnr.24833>.
 53. Nikolettou, V., Sidiropoulou, K., Kallergi, E., Dalezios, Y., and Tavernarakis, N. (2017). Modulation of Autophagy by BDNF Underlies Synaptic Plasticity. *Cell Metabol.* 26, 230–242.e5. <https://doi.org/10.1016/j.cmet.2017.06.005>.
 54. Konstantoudaki, X., Chalkiadaki, K., Vasileiou, E., Kalemaki, K., Karagogeos, D., and Sidiropoulou, K. (2018). Prefrontal cortical specific differences in behavior and synaptic plasticity between adolescent and adult mice. *J. Neurophysiol.* 119, 822–833. <https://doi.org/10.1152/jn.00189.2017>.
 55. Kalemaki, K., Velli, A., Christodoulou, O., Denaxa, M., Karagogeos, D., and Sidiropoulou, K. (2022). The Developmental Changes in Intrinsic and Synaptic Properties of Prefrontal Neurons Enhance Local Network Activity from the Second to the Third Postnatal Weeks in Mice. *Cerebr. Cortex* 32, 3633–3650. <https://doi.org/10.1093/cercor/bhab438>.

STAR★METHODS

KEY RESOURCES TABLE

| REAGENT or RESOURCE | SOURCE | IDENTIFIER |
|--|---|-----------------------------------|
| Antibodies | | |
| Rabbit Polyclonal anti-GDH2 | Homemade | Spanaki et al. 2016 ¹⁶ |
| Rabbit Polyclonal anti-GDH1 | AVIVA SYSTEM BIOLOGY | ARP45709_P050; RRID:AB_2046094 |
| Biotinylated goat anti-rabbit secondary antibody | VECTOR LABORATORIES | BA-1000; RRID:AB_2313606 |
| Fluorescein isothiocyanate-conjugated streptavidin | DAKO | F0422 |
| TRITC-conjugated anti-mouse secondary antibody | Jackson ImmunoResearch | 715-025-150; RRID:AB_2340766 |
| mouse anti insulin antibody | Thermo Scientific | Cat.#MS1379; RRID:AB_62833 |
| goat anti-mouse secondary antibody conjugated to Alexa Fluor 555 | Life Technologies/Thermo Fisher Scientific, | A-21422; RRID:AB_2535844 |
| biotinylated anti-rabbit IgG | Vector Laboratories | Cat.BA-1000; RRID:AB_2313606 |
| Mouse anti-NeuN | MILLIPORE | MAB377; RRID:AB_2298772 |
| Mouse anti-GFAP | Sigma Aldrich | SAB1405864; RRID:AB_10739114 |
| TO-PRO-3 iodide (642/661) | Invitrogen | T3605 |
| Secondary Alexa Fluoro 488 anti-rabbit IgG | Cell Signaling | Cat#4412; RRID:AB_1904025 |
| Alexa Fluoro 594 anti-mouse IgG | Cell Signaling | Cat#8890; RRID:AB_2714182 |
| PAP pen for immunostaining | MERCK (SUPELCO) | Z377821-1EA |
| Superfrost Slides 25 × 75 × 1,00mm | Thermo Scientific | J1800AMNZ |
| Cover lids 24X50mm | LABBOX | COVN-050-100 |
| OCT Compound Tissue –Tek | SAKURA | 4583 |
| Mounting Medium | DAKO | S302380-2 |
| Luminata FORTE Western HRP Substrate | MILLIPORE | WBLUF0100 |
| Bacterial and virus strains | | |
| Human BAC clone | ImaGenes, GmbH | RP11-610G22 |
| Chemicals, peptides, and recombinant proteins | | |
| Potassium dichromate | Sigma | P5271-500G |
| Mercury chloride | Sigma | 215465-100G |
| Potassium chromate | Sigma | 216615-100G |
| L-lactate | Sigma | L7022 |
| Glycine | Sigma-Aldrich | 33226-1KG |
| Phenyl-sepharose High Performance | MERCK (GE Healthcare) | GE17-1082-01 |
| Hydroxyapatite Biogel HT Gel | Biorad | 130-0150 |
| Bio-Rad Protein Assay Dye | Biorad | 5000006 |
| Protease Inhibitor Cocktail Set I, 10 vials | CALBIOCHEM | 539138-1SET |
| PageRuler™ Plus Prestained Protein Ladder, 10 to 250 kDa | Thermo Scientific™ | 26620 |
| NADPH Tetrasodium Salt | CALBIOCHEM | 481973 |
| Guanosine-5'-triphosphate disodium salt | CALBIOCHEM | 371701 |
| Adenosine 5'-diphosphate disodium salt | SIGMA ALDRICH | 01897-1G |
| Ammonium sulfate | Sigma-Aldrich | 31119-1KG |
| Ethylene glycol | Sigma-Aldrich | 102466 |
| DL-Dithiothreitol solution | Sigma | 646563-10X.5ML |
| Sodium chloride | Sigma | 71376-1KG |

(Continued on next page)

Continued

| REAGENT or RESOURCE | SOURCE | IDENTIFIER |
|---|-----------------|---------------|
| Acrylamide/Bis-acrylamide, 30% solution | Sigma | A3574-5X100ML |
| Methanol | Sigma-Aldrich | 32213-2.5L-M |
| Ethanol | Fisher Chemical | E/0650DF/17 |
| Boric acid | Sigma-Aldrich | 31146-1KG |
| Triethanolamine hydrochloride | Sigma Aldrich | T1502 |
| EDTA (TitrplexIII) | MERCK | 1.08421 |
| Dodesyl sulfate sodium salt | MERCK | 1.18309 |
| Sodium phosphate dibasic | Sigma | S9763 |
| Potassium chloride | MERCK | P9333 |
| Sodium chloride | Sigma | 71376-1KG |
| Trizma® base | SIGMA | T1503 |
| Albumin from bovine serum | Sigma | A7638-10G |
| Dimethyl Sulfoxide (DMSO) | Sigma Aldrich | D2438 |
| Agarose | Sigma Aldrich | A9539 |
| Betain solution 5M | Sigma Aldrich | B0300-5VL |

Experimental models: Cell lines

| | | |
|---|-----------------------------|---------------|
| SF21 | ECACC | Cat# 05030202 |
| BD BaculoGold Transfection Kit BV 5 transfections | BD Biosciences (Pharmingen) | 554740 |
| Culture Media | | |
| SF 900 III SFM 500ML | Life Technologies | 12658019 |
| SF 900 III SFM 1000ML | Life Technologies | 12658027 |
| FBS, QUALIFIED 100ML | Life Technologies | 10270098 |
| GRACES INSECT MED SUPPLEMENTED 500ML | Life Technologies | 11605045 |
| GENTAMICIN (50 MG/ML) | Life Technologies | 15750037 |
| EXPISF STARTER KIT EA | Life Technologies | A38841 |
| EXPISF CD MEDIUM | Life Technologies | A3767802 |
| SF 900 III SFM 500ML | Life Technologies | 12658019 |

Experimental models: Organisms/strains

| | | |
|---------------|--------------------|----------------|
| C57BL/6J mice | Jackson Laboratory | Strain #000664 |
|---------------|--------------------|----------------|

Oligonucleotides

| | | |
|---|-------------------|-------------|
| GLUD2 gene primers F:5'-TGAATGCTGGAGGAGTGACA-3' R:5'TGGATTGACTTGTTGAGAATGG-3' | Eurofins/Genomics | Custom Made |
|---|-------------------|-------------|

Software and algorithms

| | | |
|--------------------------------|--------------------------|---|
| JWatcher | UCLA | http://www.jwatcher.ucla.edu |
| IgorPro | Wavemetrics | www.wavemetrics.com |
| PanLAb Video Tracking Software | PanLaB/Harvard Apparatus | https://www.panlab.com/en/products/smart-video-tracking-software-panlab |
| Prism7 GraphPad | Dotmatics | https://www.graphpad.com/ |

Other

| | | |
|---------------------------|---------------|---------|
| Open-field chamber | custom-made | N/A |
| Fear conditioning chamber | MedAssociates | N/A |
| elevated plus maze | custom-made | N/A |
| light-dark test | custom-made | N/A |
| Glass capillaries | WPI | TW150-F |

(Continued on next page)

Continued

| REAGENT or RESOURCE | SOURCE | IDENTIFIER |
|---|-------------------|-------------|
| Stimulating electrodes | Harvard Apparatus | 72-0408 |
| Dialysis membrane Cellu-Sep T3; Nominal MWCO: 12,000–14,000 | Cellu-Sep | 1230-25 |
| Chromatography paper 3MM | Whatman | 3030917 |
| NucleoSpin Gel and PCR Clean-up, kit/250preps | MACHEREY-NAGEL | 740.609.250 |
| Porablot NCP, roll, 0,3 × 3 m, 0,45 μm | MACHEREY-NAGEL | 741280 |

RESOURCE AVAILABILITY**Lead contact**

Further information and requests for resources and reagents should be directed to and will be fulfilled by the Lead Contact, Andreas Plaitakis (andreasplaitakis@gmail.com).

Materials availability

The study did not generate new reagents.

Data and code availability

- Data reported in this paper will be shared by the [lead contact](#) upon request.
- This paper does not report original code.
- Any additional information required to reproduce the data reported in this paper is available from the [lead contact](#) upon request.

EXPERIMENTAL MODEL AND STUDY PARTICIPANT DETAILS**Ethical statement for animal experiments**

All experimental procedures including the use of the mouse model were performed according to the protocol approved by the Research Ethics Committee of the University of Crete. Animal studies were performed according to the institution and governmental guidelines and follow the European Union ethical standards outlined in the Council Directive 2010/63/EU of the European Parliament on the protection of animals used for scientific purposes. All efforts were made to minimize the number of animals and their suffering.

Experimental animals

Male *GLUD2* transgenic mice (Tg) carrying a human BAC (RP11-610G22) (ImaGenes, GmbH) clone and male C57BL/6 mice (Jackson Lab) were used for these experiments. The BAC clone, containing a 176.6 kb fragment of the human X chromosome that encompass the *GLUD2* gene along with a 40 kb of upstream and 135 kb of downstream DNA sequences, was used to construct the transgenic mice.¹² A Not I fragment of 176,610 bp was isolated from the above BAC clone and microinjected into the pronuclei of fertilized (C57BL/6J × CBA/J) F2 oocytes as previously described.¹² Microinjections and embryo implantations were carried out by Transgenics & Gene Targeting Facility at Biomedical Sciences Research Center 'Alexander Fleming'. The resulting offspring were genotyped by PCR using the primers described below.

DNA Analysis—Mouse tail DNA was extracted using the phenol/chloroform method. Founders were identified by PCR analysis using primers specific for coding sequences of the *GLUD2* gene (F: 5'-TGAATGCTGGAGGAGTGACA-3' and R:5'TGGATTGACTT GTTGAGAATGG-3'). Founders were crossed with C57BL/6 mice. F1 offspring were genotyped to identify germ line transmission using the same method. Transgenic offspring, used to maintain the transgenic line, were bred under specific pathogen-free conditions in the animal facility at Institute of Molecular Biology and Biotechnology (IMBB) of FORTH, Crete, Greece. The presence of the transgene was monitored throughout the course of the study by PCR from tail genomic DNA using the above primers. To produce heterozygous transgenic lines, *GLUD2* Tg mice were crossed with their wild-type littermates. The control mice that were used in our experiments were wild-type littermates of the *GLUD2* Tg animals. The animals were housed with 4 mice per cage in standard cages, on a sawdust bedding, at constant temperature (23 ± 2°C), humidity (55% ± 5%) and under normal 12h light/dark cycle (lights on from 7:00 to 19:00). Food and water were available *ad libitum*. Mice were killed by cervical dislocation or by inhalation of an overdose of CO₂.

Two strains (lines Tg13 and Tg32) showing comparable levels of expression of the hGDH2 protein in brain of the *GLUD2* Tg were used and studied in parallel. Adult mice of 3–6 months age were used in all experiments, except for the Golgi-Cox studies in which 15-day-old, 6 month old, 12 month old and 22 month old mice were used.

METHOD DETAILS**Western blots of brain tissue**

Crude tissue extracts were run on an 8.5% SDS-PAGE gel. Proteins were transferred on a nitrocellulose membrane and incubated with either the anti-GDH1 monoclonal antibody or the anti-hGDH2 specific polyclonal antibody. Protein bands were visualized with the use of the

ChemiLucent Detection System kit (Chemicon International, Temecula, CA). As controls we used purified wild-type hGDH1 and hGDH2 proteins, obtained by expression of *GLUD1* or *GLUD2* cDNA in Sf21 cells using the baculovirus expression system.¹³

Brain slice preparation

All animals were deeply anesthetized using pentobarbital sodium (60 mg/kg, i.p) and then perfused with 30 mL PBS followed by 30 mL 4% paraformaldehyde (PFA). The brains were removed immediately after perfusion and fixed in 4% PFA for 40 min. Upon fixation, tissues were sucrose cryoprotected (30% sucrose in phosphate buffer, pH 7.4) and embedded in gelatin (7.5% gelatin/15% sucrose in phosphate buffer, pH 7.4) and then were snap-frozen by exposure to isopentane. Coronal serial sections were obtained via cryotome and transferred to gelatin coated glass slides (or in positively charged SuperFrost slides, ThermoFischer Scientific).

Double immunofluorescence staining

Brain sections were fixed in acetone for 8 min. Non-specific binding sites were blocked at RT for 40 min in 5% BSA in 0.5% Triton X-100 PBS and then incubated with at 4°C for 18h with rabbit primary antibodies recognizing either hGDH1 or hGDH2 protein and with mouse primary antibodies for NeuN, GFAP. After 3 washes in PBS, incubation with fluorescence-labeled secondary antibodies was performed with biotinylated goat anti-rabbit secondary antibody followed by Streptavidin FITC or goat anti-mouse Alexa Fluor 555 secondary antibody. Nuclei were visualized with TOPRO. Visualization was performed using a Leica Confocal microscope.

Golgi-Cox staining

The Golgi-Cox procedure was performed as published previously.^{52,53} The brains of *GLUD2* and Wt mice were removed and placed in Golgi-Cox solution (5% Potassium Dichromate, 5% Mercuric Chloride (sublimite), and 5% Solution of Potassium Chromate), which had been prepared at least 5 days earlier. Brains remained in Golgi-Cox solution for 10 days at room temperature, then placed in 30% sucrose solution and subsequently sliced (150 mm thick slices) in a vibratome (Leica VT1000S). The slices were placed onto gelatin-coated microscope slides, covered with parafilm, and maintained in a humidity chamber for about 30–40 h. The parafilm was then removed, and the slides were incubated first in ammonium hydroxide for 15 min in a dark room and then in Kodak Fix solution for 15 min followed by washes with H₂O. The brain slices were then dehydrated with increasing concentrations of ethanol, incubated in xylene for 5 min and cover-slipped with permount. The slides were kept for at least two months before imaging under the 100X lens of a Nikon Eclipse E800 microscope. Secondary dendritic segments of 30–40 mm length from 4 to 5 neurons in the CA1 and another 4–5 neurons from the CA3 area from each animal were analyzed for the number of dendritic spines. Measurements differentiated between mushroom and stubby spines based on the presence of a neck for the mushroom spines (Figure 3A). The number of mature (mushroom and thin) and stubby spines were measured on different secondary dendritic segments from each animal and spine density was calculated; 3–5 segments were measured from each animal. Statistical comparisons were performed with unpaired t-test.

Electron microscopy

Anesthetized Tg and Wt animals were perfused with 2% glutaraldehyde and 2%PFA in 0.1 M phosphate buffer (PB), pH 7.3. The brains were removed and transferred in the same fixative overnight. Brain slices (400μm) were taken using a vibratome (Leica 1000VT) and the CA1 region was micro dissected under a stereoscope. The dissected hippocampi were post-fixed in 1% osmium tetroxide for 1 h, dehydrated with increasing concentrations of ethanol and embedded in epoxy resin (Durcupan ACM, Fluka). Ultrathin sections (70–80 nm) were obtained using the EM UC6 (Leica) ultramicrotome, contrasted with lead and viewed using a transmission electron microscope (100C, JEOL) operating at 80 kV. For the analysis, 10–20 randomly chosen electron micrographs of the Schaffer collateral layer were obtained at 80,000 magnification for each animal. In total, 6 animals were used for analyses: 3 Wt and 3 Tg animals. Synapses were imaged at 40000X and 80000X magnification. The numbers of synapses in each different micrograph were analyzed and an average was computed for each animal.

Electrophysiology

Slice preparation

Electrophysiological experiments were performed using the *in vitro* slice preparation, as published previously.^{52–55} Wt and *GLUD2* Tg mice (4–5 months old) were decapitated under halothane anesthesia. The brain was removed immediately and placed in ice-cold, oxygenated (95% O₂/5% CO₂) artificial cerebrospinal fluid (aCSF) containing (in mM): 125 NaCl, 3.5 KCl, 26 NaHCO₃, 1 MgCl₂ and 10 glucose (pH = 7.4, 315 mOsm/l). The brain part containing the hippocampus was blocked and glued onto the stage of a vibratome (Leica, VT1000S, Leica Biosystems GmbH, Wetzlar, Germany). 400μm thick brain slices containing the hippocampus were taken and transferred to a submerged chamber, which was continuously superfused with oxygenated (95% O₂/5% CO₂) aCSF containing (mM): 125 NaCl, 3.5 KCl, 26 NaHCO₃, 2 CaCl₂, 1 MgCl₂ and 10 glucose (pH = 7.4, 315mOsm/l) in room temperature (namely control aCSF). Slices were then transferred to a submerged recording chamber, which continuously superfused oxygenated (95% O₂/5% CO₂) aCSF containing (in mM): 125 NaCl, 3.5 KCl, 26 NaHCO₃, 2 CaCl₂, 1 MgCl₂, 10 glucose (pH = 7.4, 315mOsm/l) at room temperature.

Field excitatory postsynaptic potential recordings

Extracellular recording electrodes filled with NaCl (2M) were placed in the stratum radiatum (SR) layer of the CA1 region. Platinum/iridium metal microelectrodes (Harvard apparatus UK, Cambridge, UK) were also placed in the SR layer, about 300 μ m away from the recording electrode, and were used to evoke fEPSPs. The voltage responses were amplified using a Dagan BVC-700A amplifier (Dagan Corporation, Minneapolis, MN, USA), digitized using the ITC-18 board (Instrutech, Inc) on a PC using custom-made procedures in IgorPro (Wavemetrics, Inc, Lake Oswego, OR, USA). The electrical stimulus consisted of a single square waveform of 100 μ sec duration given at an intensity that generated 40% of the maximum fEPSP, using a stimulator equipped with a stimulus isolation unit (World Precision Instruments, Inc).

Data were acquired and analyzed using custom-written procedures in IgorPro software (Wavemetrics, Inc, Lake Oswego, OR, USA). The voltage response was analyzed in order to measure the fEPSP slope. Baseline responses were monitored for at least 10 min, then two theta-burst trains (5X 4spikes at 100Hz) with an inter-stimulus interval of 20 s were applied and finally responses were acquired for 30 min post-tetanus. In some experiments, 10 μ M of D-lactate was added to the aCSF 20 min prior to theta-burst stimulation and until 20 min after the theta-burst stimulation. The fEPSP slope of each response was normalized to the average 10 min pre-tetanic average fEPSP slope. Statistical analyses were performed by repeated measures ANOVA.

Spontaneous local field potential (LFP) recordings

Spontaneous LFP traces were acquired for 10 min before the beginning of the baseline responses for the LTP protocol. In order to identify spontaneous events, the standard deviation of background signal was calculated in the 'quiet' part of each voltage response trace. As a spontaneous event was identified any voltage response larger than the average background voltage plus four times the standard deviation of the background signal. The number of spontaneous events was averaged for each sample for the 10 min period. Statistical analysis was performed with an unpaired t-test.

Patch-clamp recordings: Data acquisition

Neurons were impaled with patch pipettes (5–7 M Ω) and recorded in the whole-cell configuration in the voltage-clamp mode. For voltage-clamp experiments, the composition of the intracellular solution was: 120 mM Cs-gluconate, 20mM CsCl, 0.1 mM CaCl₂, 1 mM EGTA, 0.4 mM Na-guanosine triphosphate, 2mM Mg-adenosine triphosphate, 10 mM HEPES. Whole-cell measurements were low-pass filtered at 5 kHz using an Axopatch 200B amplifier (Molecular Devices, Inc). Recordings were digitized with the ITC-18 board (Instrutech, Inc) on a PC using custom-made codes in IgorPro (Wavemetrics, Inc). All signals were collected at a sampling frequency of 20kHz. Five second recordings were taken either at –60mV or at +20mV for the detection of sEPSCs and sIPSCs, respectively. To measure sNMDA currents, 10 μ M bicuculline was superfused in the aCSF and recordings were taken at +30mV. Data Analysis: Data were analyzed using custom-written codes in IgorPro software (Wavemetrics, Inc). The measurements of sEPSCs were taken at –60mV and sIPSCs at +20mV and the measurements of sNMDA currents at +30mV following addition of bicuculline. Automatically selected events were subsequently visually monitored to discard erroneously included noise. All currents detected from every single neuron were averaged. The peak amplitude was calculated as the maximum current value in each trace (5s duration) and averaged for all traces of a single neuron.

Behavioral experiments

Attention set-shifting task

Mice were handled by the experimenter and food-restricted to 85–90% their initial weight before the start of the experiment. Mice were habituated to the test chamber and were trained to dig through the bowls in order to get their reward. In the first stage (simple discrimination, SD) of the task two different bedding materials were provided (smoking pipe cleaning rod and silver thread) one of which had the reward. In the second stage (compound discrimination, CD), a new dimension was introduced using two different odors (strawberry and lavender). During this stage, the same substrate still remains relevant to the reward while the odors are irrelevant. The third stage (compound discrimination reversal, CDR) uses the same substrates and odors as the second phase, but the reward is now in the other substrate. During the fourth stage (interdimensional shift I, IDI), two new digging media (cardboard and wool) and two new odors (jasmine and apple) are introduced. One of the digging media is still the relevant variable in this phase. The next stage (interdimensional shift II, IDII) uses again two new substrates (colorful gobbled paper and cotton) and two new odors (vanilla and cherry). This time the gobbled paper is the rewarded digging media. In the 6th stage (interdimensional reversal, IDR), the correct and the wrong digging media are reversed while vanilla and cherry odors are irrelevant to the reward. In the last stage (extradimensional shift, EDS), the reward now is governed by the odors. The digging media (confetti and cloth) and the odors (ocean and freesia) used in this stage are introduced for the first time in this experiment. These experiments were performed in both Tg32 and Tg13 lines. Statistical analysis was done using one-way ANOVA. A p value of less than 0.05 is deemed to be statistically significant.

Contextual fear conditioning/extinction task

Wt and *GLUD2* male mice, 5-months-old, were placed in the fear conditioning chamber (MedAssociates, St. Albans, VT, USA), which was controlled through a custom-made interface connected to the computer. After 7 min of habituation to the conditioning chamber, each mouse received one mild electrical foot shock (1000 m, 0.75 mA), and remained in the chamber for another 5 min. The following day, mice were returned to the training chamber using the same context for 10 min. The same procedure was repeated for another 4 days. The freezing

behavior was analyzed manually using the J-Watcher software (<http://www.jwatcher.ucla.edu>). These experiments were performed in both Tg32 and Tg13 lines. Statistical analysis was done using non parametric two sample t-test and one-way ANOVA. A p value of less than 0.05 is deemed to be statistically significant.

Left-right discrimination (reference memory)

The T-maze apparatus used includes a start arm and two goal arms (45 × 5cm each). The left-right discrimination task examines reference memory in mice. Mice were initially handled by the experimenter for about a week, and then habituated in the T-maze apparatus, for 2 days. Mice were food-deprived in order for food to serve as a potent reinforcer. The feeding regime was adjusted in such a way that the animals maintained 85–90% of their initial weight. During the second habituation day, the time that each mouse spent in each arm was calculated in order to establish the arm preference for each mouse. All mice were trained in the left-right discrimination task for 1 day. Each mouse, individually, was subjected to a single 20-trial session and trained to look for the reward on the arm opposite to the preferred one, as identified in the second habituation day. These experiments were performed in both Tg32 and Tg13 lines. Statistical analysis was done using non parametric two sample t-test and one-way ANOVA. A p value of less than 0.05 is deemed to be statistically significant.

The elevated plus maze test

The elevated plus maze apparatus consists of four narrow arms arranged around a small central area in a plus (+) shape. The two opposite arms are enclosed with walls while the other two arms remain open and exposed. The maze is elevated above the floor. Test animals are allowed to freely explore the maze for a single 5 min period while their behavior is recorded using a video camera mounted above the maze. The preference for being in open arms versus closed arms is calculated to measure anxiety-like behavior. Statistical analysis was performed using non-parametric two sample t-test and one-way ANOVA (Prism7 GraphPad Software). A p value of less than 0.05 is deemed to be statistically significant.

The light/dark test

The apparatus has two connected compartments (48 cm × 24 cm × 27 cm in total). One compartment is lightened and of white color (aversive area) and the other is darkened and of black color (safe area). An opening interconnects the two compartments. Test subjects are placed in the light area and begin moving throughout the compartment until they locate the opening to the dark area. Mice are allowed to move freely between the two chambers. The time the animal spent moving, rearing and transitioning from the light to dark compartment was recorded for a 10 min period using the SMART Video Tracking camera and software (PanLab/Harvard Apparatus) and then statistically analyzed using non-parametric t-test and one-way ANOVA (Prism7 GraphPad Software). A p value of less than 0.05 is deemed to be significant.

Sensitivity to thermally induced pain

For assessing thermal pain sensation, we employed two different protocols that use an external stimulus to elicit a withdrawal response of animal's plantar: hot plate and the plantar test (Hargreave's method). In the hot plain test, mice (unrestrained) were placed on a metal surface maintained at the constant temperature of 54°C and the response latency (hind paw withdrawal or licking) is recorded by the experimenter. To prevent tissue-damage a pre-determined cut-off time had been set. During the Hargreave's test (Plantar test apparatus Ugo Basile, Varese, Italy) an infrared heat stimulus is applied to the plantar surface of test subjects which are unrestrained. The apparatus consists of six chambers which are placed on a transparent glass pane. Instrument acclimation for a six-day period is required. During testing, time latency (paw withdrawal) is recorded automatically by a fiber optic sensor. For each group of testing subjects the mean of reaction time was calculated and the obtained values were statistically analyzed using nonparametric t-test and one-way ANOVA (Prism7 GraphPad Software). A p value of less than 0.05 is deemed to be statistically significant.

Object location task (spatial memory)

The test is based on the inherent preference of mice for novelty. Testing occurred in an open field box with opaque walls (43 cm × 33cm × 43), to which -already handled-animals are first habituated (no item is introduced to test subjects during the habituation period) for 10 min for a 3-day period. On testing day, during the trial phase mice are allowed to explore the arena and the objects freely for 10 min. One hour later the animal is re-introduced for 10 more minutes to the open field arena, where the one of the two objects of trial had changed position (test phase). Both trials are recorded using a camera mounted above the arena. After each session the used objects and the open field arena are cleaned with 70% ethanol. Data analysis is performed by calculate the interaction time of mice with each object during the trial and the test phases. Performance of the animals is evaluated via a discrimination index ($DI = (N - F) / (N + F)$ (N = time spent in object in the novel location, F = time spent in object in the familiar location). Any emerging differences in the performance of the testing groups were determined using non parametric t-test and one-way ANOVA (Prism7 GraphPad Software). A p value of less than 0.05 is deemed to be statistically significant.

Object recognition task (recognition memory)

The test is based on the same principle as the Object location task and is identical to the aforementioned test except that during the test phase one of the familiar objects (that the mice were initially introduced to) had been replaced by a novel object. Measurements were

made at 5 min and at 10 min. The animal's preference for the novel object versus the familiar object is determined by the Discrimination Index ($DI = (N - F) / (N + F)$) with N the time spent in novel object and F the time spent in the familiar object. Statistical analysis was performed using two sample t-test and one-way ANOVA. A p value of less than 0.05 is deemed to be statistically significant.

Spontaneous locomotor activity

The open field maze consisted of a square, transparent PVC wall-enclosed area (41 cm × 33cm x 41 cm, Ugo Basil, Varese, Italy), with photocell emitters and receptors equally spaced along the perimeter of the chamber. The horizontal movement of the test subject causes beam breaks which then are analyzed. For a more detailed accession of the animal locomotor activity and behavior an SMART Video Tracking camera and software were used (PanLab/Harvard Apparatus). Animals were allowed to move freely in the chamber for 45 min per day during a 3-day habituation period. On the 4th day, their horizontal locomotor activity was recorded for a single 60 min period. The mean of horizontal activity (units) was analyzed and calculated for each group (Wt and Tg) and statistical analysis of the obtained data was performed using non parametric two sample t-test and one-way ANOVA (Prism7 GraphPad Software). A p value of less than 0.05 is deemed to be statistically significant.

QUANTIFICATION AND STATISTICAL ANALYSIS

Brain morphological analysis

Dendritic spine density (Golgi Method) was quantitated in hippocampal slides from Tg and Wt mice by measuring the number of spines in secondary dendritic segments of 30–40 μm length from 4 to 5 neurons in the CA1 and another 4–5 neurons from the CA3 area from each animal. Measurements differentiated between mushroom and stubby spines based on the presence of a neck for the mushroom spines (Figure 3A). The number of mature (mushroom and thin) and stubby spines was determined in different secondary dendritic segments; 3–5 segments were measured in each animal. An average number was computed for each animal and statistical comparisons were performed using the unpaired t-test. *Synaptic density* was studied using Electron Microscopy. Synapses were imaged at 40,000X and 80,000X magnification. Quantitation was performed by measuring the number of synapses present in 10–20 randomly chosen electron micrographs in the Schaffer collateral layer (obtained at 80,000 magnification) for each animal. An average number was computed for each animal and statistical comparisons were done using the t-test.

Electrophysiological studies analysis

To evoke fEPSPs, we used an electrical stimulus (consisting of a single square waveform of 100 μsec duration), the intensity of which was adjusted to generate 40% of the maximum fEPSP. The voltage response was analyzed in order to measure the fEPSP slope. Baseline responses were monitored for at least 10 min, then two theta-burst trains (5X 4spikes at 100Hz) with an inter-stimulus interval of 20 s were applied and finally responses were acquired for 30 min post-tetanus. The fEPSP slope of each response was normalized to the average 10 min pre-tetanic average fEPSP slope. Statistical analyses were performed by repeated measures ANOVA. To identify spontaneous events, the standard deviation of background signal was calculated in the 'quiet' part of each voltage response trace, and any response larger than the average background voltage plus four times the standard deviation of the background signal was identified as spontaneous event. For each sample, the number of spontaneous events for 10 min was averaged and statistical comparisons were done using the unpaired t-test.

Behavioral experiments analyses

Attentional set-shifting memory was quantitated by computing the "total # of trials" to criterion (6 consecutive correct trials). Regarding the freezing behavior observed during the contextual fear conditioning, this was analyzed manually using the J-Watcher software (<http://www.jwatcher.ucla.edu>). During the light/dark test, the time the animal spent moving, rearing and transitioning from the light to dark compartment was recorded for a 10 min period using the SMART Video Tracking camera and software (PanLab/Harvard Apparatus) Results of all behavioral experiments are given as mean values ± SE. Independent samples t-tests were used to compare continuous variables between the Tg and Wt groups and one-way ANOVA. Also, one-way ANOVA was used to evaluate differences between the three mice groups (Tg13, Tg32, Wt). Repeated measures ANOVA was used to evaluate the different in LTP experiments. Post-hoc Bonferroni adjusted tests were used to pinpoint differences. p values <5% was the criterion for significance. All analyses were performed using the IBM-SPSS 25. Graphical representations were done using the GraphPad Prism 7.